Cloud-base heights over different land-use classes

Learnings of a distributed Logtag network in and around the Guatemalan cloud forest

CEGM3000: Multidisciplinary Project

Cloud Chasers V

Delft University of Technology

TU Delft

MDP Cloud Chasers V

Cloud Forest Sensor Netowrk

Cloud Chasers V

October 2025

Report submitted for the Multi-Disciplinary Project CEGM3000

Pooja Trivedi	6296327
Johannes van Hooff	5171431
Alma Sierra Delgado	6315860
Klaas Laan	5279658
Collin Smook	6298036
Bob van Daal	5172802

Supervisors: Prof.dr. Miriam Coenders
Prof dr. Marc Schleiss
Prof dr. Ruud van der Ent
Linnaea Cahill

Abstract

Cloud forests play a critical role in regulating regional hydrology through fog interception, biodiversity support, and groundwater recharge. However, increasing deforestation and land-use change threaten the functionality of these ecosystems, partially by altering cloud formation processes. This study investigates how different land-use types affect cloud base height (CBH) in the Mestelá River catchment in Alta Verapaz, Guatemala. Using a distributed sensor network of temperature, humidity, and pressure sensors deployed across cloud forest, pine forest, and agricultural land, vertical profiles were collected over multiple field campaigns.

Cloud base height was estimated through a lifting condensation level (LCL) model based on local atmospheric measurements. Results show systematic differences between land-use types: cloud forests exhibited cooler and more humid conditions, resulting in a lower CBH compared to pine forests and open agricultural areas. Open fields consistently showed the highest daytime temperatures and lowest relative humidity, producing the highest estimated cloud bases. Pine forests exhibited intermediate conditions.

These microclimatic differences were incorporated into the FIESTA fog interception model, improving spatial and temporal representation of fog occurrence and interception efficiency. It was shown that especially improving the temporal accuracy of FIESTA inputs by forcing a diurnal pattern led to more accurate results. In addition, a simplified canopy water balance model was applied to evaluate the hydrological contribution of fog events at stand level. The results confirm that land-use change alters cloud immersion frequency and potentially reduces dry-season water inputs in deforested areas.

This study demonstrates that deforestation influences atmospheric processes at local scales with direct hydrological consequences, underscoring the importance of cloud forest conservation for water security in mountainous regions. The deployed sensor network and modeling framework offer a scalable method for monitoring cloud dynamics and evaluating land-use impacts in other tropical montane systems.

Summary

Cloud forests in Alta Verapaz, Guatemala form a vital component of regional water supply by intercepting fog and regulating microclimates. Rapid expansion of agriculture and pine monoculture has transformed large parts of the landscape, raising concerns about changing cloud dynamics and potential impacts on downstream water availability.

This project aimed to quantify how land use affects cloud base height by installing a distributed network of air temperature, humidity, and pressure sensors across different vegetation types. Data were collected in five measurement batches covering cloud forests, pine plantations, agricultural fields, and mixed forest areas. Using these observations, cloud base height was estimated through a physically based lifting condensation level model.

The analysis demonstrates a clear land-use signal in atmospheric conditions. Cloud forest areas were generally cooler and more humid, leading to a lower cloud base. Pine forests were warmer and less humid, while agricultural land exhibited the warmest and driest conditions, producing the highest estimated cloud bases. These differences were most pronounced during daytime, which plays the dominant role in cloud formation and atmospheric instability.

To investigate hydrological consequences, local cloud base estimates were integrated into the FIESTA fog interception model. Three steps were undertaken to improve accuracy of modeled lifted-condensation-level values. Firstly, land-use dependent correction factors for temperature and humidity were implemented. Secondly, a simplified method for calculating the LCL was replaced by a more robust iterative approach. Thirdly, the diurnal pattern that was present in the measurements and calculations using the LogTag network was reinforced into the FIESTA model through a diurnal pattern inside the forced RH data. This led to an increase in realism and sensitivity to deforestation scenarios. In parallel, canopy water balance calculations based on tower measurements demonstrated that fog events provide a non-negligible water input to forest systems, especially during periods of limited rainfall.

Beyond biophysical findings, the study emphasizes socioeconomic implications: many communities depend directly on cloud-derived water sources, yet face increasing water insecurity due to ecosystem degradation and failing infrastructure. Field observations and interviews revealed strong links between land use, water quality, agricultural practices, and public health.

Overall, this project provides quantitative evidence that deforestation affects cloud formation processes and reduces the hydrological resilience of the catchment. It highlights the importance of integrating atmospheric science into water management strategies and supports the role of agroforestry and forest conservation as climate adaptation measures.

Acknowledgements

This multidisciplinary project came to life through the support and generosity of many people and organisations.

We are grateful to Students for Sustainability and the FAST Fund for making the fieldwork possible in the first place.

In Guatemala, CCFC, Rob and Tara Cahill provided invaluable guidance, together with Luis who kept us safe from sometimes dangerous local wildlife.

We want to thank all the girls at CCFC and Ludwin for welcoming us into their community and helping us navigate both the forest and the logistics behind it.

We would also like to thank our supervisors at TU Delft for their patience and insights throughout this project. A special thanks goes to Linnaea for her constant support and for being so involved, many thanks for how available you were and your constant interest!

Finally, we are deeply grateful to Ariel and his family, who opened up their land to our research and by doing so gave us an unforgettable experience.

Contents

1. Introduction

1.1. Problem Definition

Cloud forests play a vital role in the global ecosystem by providing critical habitats for countless species of plants and animals [1], providing water to nearby towns and cities, and helping regulate local and global climates. Due to their unique ability to capture moisture directly from clouds, these forests are a key component of the hydrological cycle [2].

Although cloud forests cover only a small fraction of the Earth's surface, their extent is rapidly declining due to deforestation, agricultural expansion, and climate change [3], [4]. Because the ecological and hydrological processes within cloud forests are not yet fully understood, it remains difficult to predict the exact consequences of this loss. However, existing research suggests that the disappearance of these ecosystems has severe impacts on biodiversity, water availability, and climate regulation [5], [6].

One of the potential atmospheric consequences of deforestation is an increase in cloud base height, the altitude at which water vapor condenses and cloud formation is initiated [7]. Deforestation can locally raise this condensation threshold by changing land–atmosphere interactions such as air temperature or relative humidity at the surface.

These mechanisms are particularly critical in tropical and montane cloud forests, ecosystems where a proportion of the local hydrological budget depends on water collection from clouds and mist. Cloud forests are capable of capturing water directly from low clouds via foliage, epiphytes, and bryophytes, symbiotic and structurally specialized vegetation types capable of direct cloud-water collection [3]. If the cloud base rises consistently above the height of the forest canopy this results in a reduced capacity of the ecosystem to collect moisture from the atmosphere. This can constrain total water availability and weaken cloud-forest resilience.

Concluding, the loss of cloud forests has a profound effect on regional biodiversity and local hydrological functioning. Alteration in the available atmospheric water and disruptions of the regional water balance directly influences the local water sources where many communities depend on. This indicates the additional socioeconomic implication deforestation may have. Therefore, it is essential to map and assess the relationship between deforestation and the needs of ecosystems and local communities. This project focused on the basics of this by studying the effects of land use types on atmospheric processes that are important for the hydrological system.

1.2. Research Objective and Hypothesis

The objective of this study is to contribute to the hydrological understanding of cloud forests, with an atmospheric focus. The project examines how different land-use types influence

cloud formation.

Tree cover cools the local climate through shading and evapotranspiration. Previous observational and modeling studies have shown temperature rising induced by deforestation of montane forests of 0.6°C - 3°C [7], [8], [9]. This warming effect of deforestation is related to an increase of the cloud base height as warmer temperatures will cause higher lifting condensation level at the same humidity [7], [10]. Scholl et al. (2021) shows the importance of vegetative cover as a decreased evaporative fraction rises sensible heat fluxes and cloud base height [11]. A higher cloud base height might therefore be the result of the lower evaporative fraction of agricultural land and pine monocultures compared to cloud forests.

Accordingly, we hypothesize that the conversion of cloud forests to agricultural land or pine monocultures leads to increased local temperatures, reduced relative humidity, and elevated cloud base height. Temperature and humidity sensors spread over different terrains will generate the data to calculate the cloud base height. The results obtained from the sensors will additionally be used to evaluate their potential to enhance a local fog interception model. Given the importance of cloud forests for regional water resources, this study highlights the critical need to preserve these ecosystems, especially on small local scales.

1.3. Collaboration with Community Cloud Forest Conservation

Conservation of these cloud forests is one of the main goals of Community Cloud Forest Conservation (CCFC), a non-profit organization that focuses on nature conservation and community development. To protect Guatemala's cloud forests, CCFC aims at cloud forest reforestation and the stimulation and education of local communities. By increasing environmental awareness and restoring deforested areas, CCFC promotes both ecological preservation and the resilience of local communities.

This project is a collaboration between CCFC and students at TU Delft that aims to improve the understanding of hydrological processes within a cloud forest. This knowledge is of great value to CCFC as it supports their goal to raise environmental awareness and provide effective education within the region.

1.4. Continuation of Previous Collaborations

With a focus on atmospheric sciences and hydrology, this project builds upon previous collaborations between CCFC and student teams from TU Delft. Over the past several years, these student groups, known as the 'Cloud Chasers', have worked to expand understanding of the hydrological cycle in the Cobán watershed. These former projects included studies on water security and the role of fog, canopy, and river discharge measurements with hydrological modeling, scenario testing for land-use change, and the construction of a monitoring tower combined with community engagement for conservation.

Where CCV distinguishes itself is in the fact that its focus lies slightly more on the atmospheric science side. Some elements from previous groups are explicitly used, such as using data provided by the tower that CCIV constructed and the modeling framework of CCIII

2. Contextualizing the project

In this chapter we will discuss the geographical, socio-economic and hydrologic setting in which our project took place.

2.1. Study Area: Mestelá River Catchment, Alta Verapaz

This project is conducted at the Community Cloud Forest Conservation (CCFC), located in the Alta Verapaz region, a department in the northern central part of Guatemala.

Figure 2.1.: Alta Verapaz ([12])

Within the Alta Verapaz region, several watersheds can be found. This project focuses on the Cahabón watershed, with particular attention to the Mestelá River catchment. The river originates in the San Pablo Xucaneb region, flowing through a variety of terrains such as open river sections, caves, and stretches of underground flow before joining the Cahabón River in the city of Cobán.

The Mestelá River Catchment is the main water source to the city of Coban, providing nearly 50% of its total water supply. The catchment is characterized by a significant elevation difference over a relatively short distance. It ranges from 2600m a.s.l. to 1400m a.s.l., within

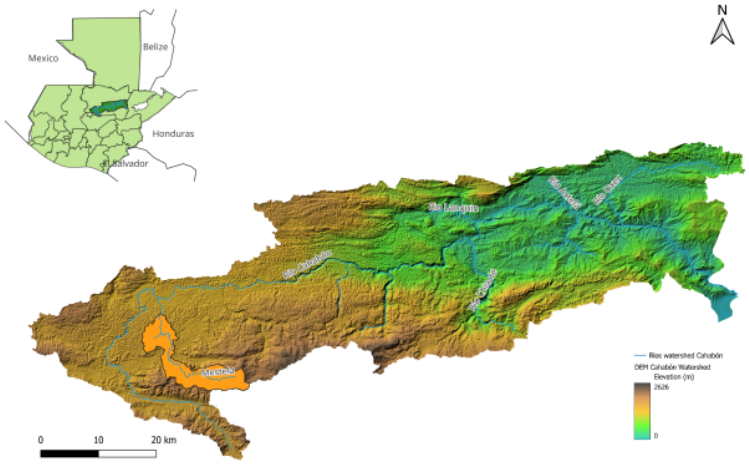

Figure 2.2.: The Cahabon watershed & Mestelá catchment [13]

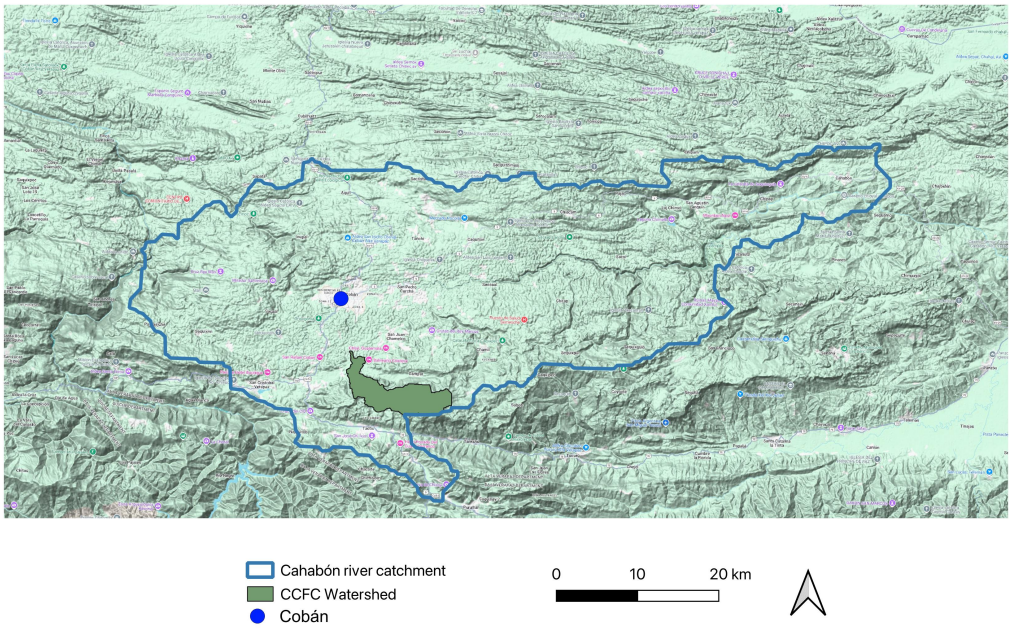

Figure 2.3.: The location of CCFC inside the Cahabon catchment

17 kilometers, with most of the elevation drop being in the most southern part of the catchment, as shown in Figure 2.4 [14].

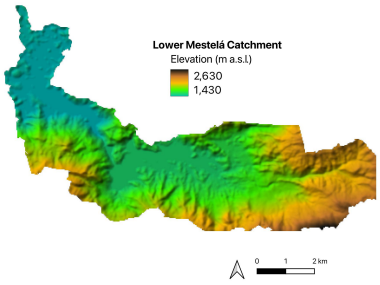

Figure 2.4.: An elevation map of the Lower Mestela catchment

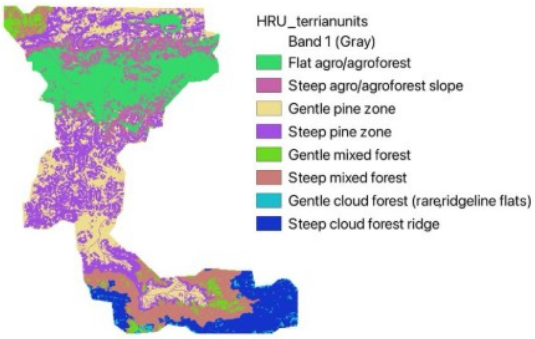

Figure 2.5.: Classified Hydrological Response Units for Mestela Catchment

Historically, the natural vegetation in the catchment consisted of cloud forest, but its extent has declined significantly over the past decade, with the landscape being increasingly dominated by large areas of pine monocultures and agricultural land [14].

2.2. Land Use Types

The Mestelá Catchment is characterized by a diverse range of land types. This chapter discusses the most prominent land types: villages, cloud forest, pine forest, and agricultural areas. In addition, the currently ongoing changes in land use and land use change over the past decades will be discussed.

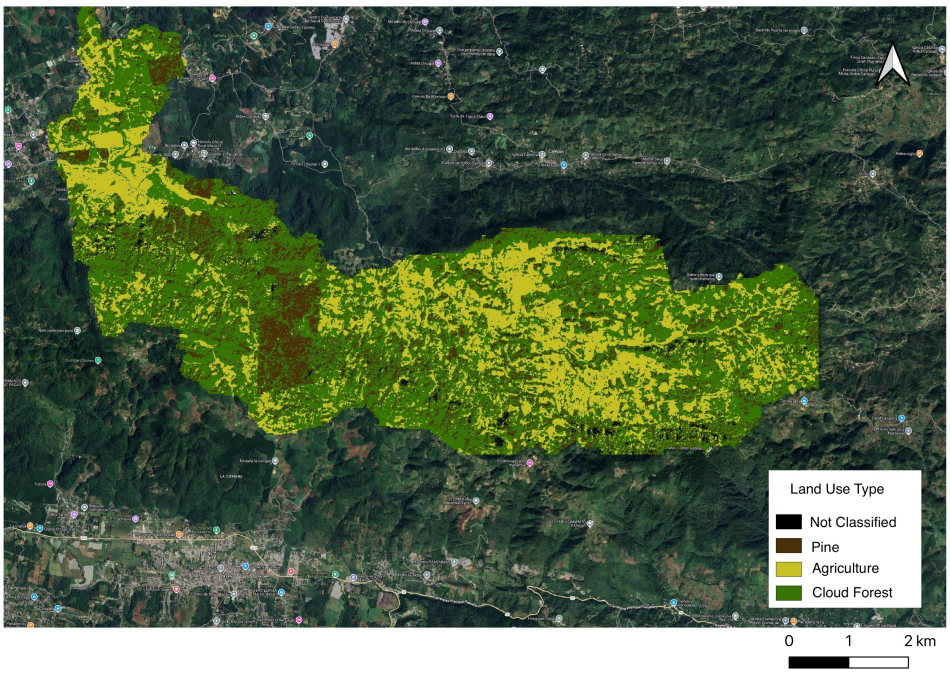

Figure 2.6.: SCP Land Use clasifications

2.2.1. Villages

Only a small portion of the land in the Mestelá Catchment is occupied by small villages. In these villages the Q'eqchi' live, the predominant Maya group in Guatemala [15]. Their livelihood largely depends on agriculture, which is the biggest land use type in the region [14]. Poverty levels in the villages are high. Access to (secondary) education is very limited. Households are increasingly dependent on local natural resources, which drives up the pressure on surrounding forests [16].

Most Q'eqchi' communities in the catchment rely on nearby springs and streams for their water for drinking and daily use. An significant water infrastructure is scarce, making the households very sensitive to changes in lang use and forest cover in the Mestelá Catchment [17].

2.2.2. Cloud Forests

As shortly mentioned in the previous chapter, cloud forests, also known as montane rain forests, historically are the natural vegetation in the Mestelá River Catchment. Cloud forests can typically be found on steep mountain slopes at elevations between 1,200 and 3,000 meters above sea level [18]. These forests are characterized by the almost constant presence

of mist or low-level clouds. This presence allows for direct water collection from the atmosphere through leaves, mosses, and epiphytes. This process is known as fog interception or horizontal precipitation (more on this in chapter 2.3). The intercepted water drips on the forest floor, infiltrates the ground, replenishes groundwater, and feeds streams and rivers. This slow infiltration process protects the land against soil erosion and helps stabilize mountain slopes. [19]

The persistent moisture created by these hydrological processes also maintains a high diversity of plant and animal species. High humidity levels, moderate temperature, and dense vegetation provide a unique climate that functions as a specific habitat for epiphytes, birds, amphibians, and numerous endemic organisms. Therefore, cloud forests are regarded as biodiversity hot spots. [20]

Cloud forests are essential for the Q'eqchi' villages, because they are their primary source of water in the region. The fog interception keeps the springs in the area flowing, even during longer periods of drought. Also, the dense root networks of cloud forests provide slope stability for the soil on the steep slopes surrounding the Q'eqchi' villages [13].

2.2.3. Pine Forests

The second main vegetation in the region are pine trees. [21] States that the elevation of cloud forests varies around the world, roughly between 1200 and 3000 m.a.s.l. In our area of study, pine forests generally are present below the cloud forest, so under 1800m a.s.l. [17]. They are also more likely to appear on slopes facing the south, where there is generally more sun and less precipitation [18].

Pine forest are mainly monocultural and lack undergrowth, compared to cloud forests. They contain very few epiphytes and mosses, which drastically reduces their ability to intercept fog. It also limits water storage within the vegetation [13].

Pine forest in the area are also subject to ongoing (small-scale) disturbances. Satellite observations indicate selective logging as well as clearing for agricultural expansion. These activities thin the canopy, increase runoff, enhance soil erosion, and contribute to greater hydrological variability in the catchment [14].

Pine forests are of importance for the Q'eqchi' households, for multiple reasons. The cutting of trees is common, since it is used as their only domestic fuel for cooking and heating. Furthermore, pinewood is widely used as a building material [14]. Additionally, large pine plantations are grown in the catchment, for economic purposes, serving as a valuable income source [13].

2.2.4. Agricultural land

The largest portion of land in the Mestelá River Catchment consists of agricultural land, roughly 47% [13]. Agriculture is very important to the Q'eqchi' communities. Most families in the region have a small-scale agricultural farm where they farm maize and beans. Corn (maize) is at centre of the Q'eqchi' diet, farming system and thus also at the centre of Q'eqchi' culture. Each meal throughout the day is based on maize and beans and families typically have a farm just large enough to produce sufficient food for their families. [22]

Population growth and the resulting agricultural expansion are the main drivers of deforestation in Alta Verapaz, which now also happens on steep slopes [13]. Combined with the fact that the fallow periods become shorter, which leads to soil degradation and increased erosion, the grade of infiltration and water storage capacity keeps decreasing in the region [14]. The result is that agricultural land is both a foundation of Q'eqchi' livelihoods and a major driver of environmental change.

(a) Cloud Forest (b) Pine Forest (c) Agricultural ([13])

Figure 2.7.: Cloud Forest, Pine Forest & Agricultural land types

2.2.5. Deforestation

As mentioned before, the historical main vegetation type in the Alta Verapaz region consisted of cloud forest. This situation began to change around the 1950s, when migration and population growth increased. This is when deforestation of cloud forest started. However, the rate of deforestation has since accelerated. The annual loss of cloud forest between 1987 and 1995 was 1.1% [14], but it now is approximately 1.9% for the period 2014–2023 [13]. The main reasons for this growing deforestation rate are increasing economic pressure on farmers and continued population growth.

Q'eqchi' households largely depend on growing corn and also somewhat on timber extraction [22]. While land is subdivided among children each generation, with poverty being high, off-farm income being limited, and with a growing population, more and more people need farmland simply to survive. As a result, the first stage of deforestation is often degradation. Because the remaining cloud forest is mostly located on steep slopes and at high altitudes, completely clearing a patch is challenging, so people turn to selective logging of the most valuable and accessible trees, fuelwood extraction, small clearings and trails, and, in some cases, planting pine in or near cloud forest [23].

Some of the consequences of degradation are opening of the canopy, a decrease in the amount of epiphytes and mosses, and less fog interception. This then makes the forest drier and warmer. Additionally, it leaves soils more vulnerable to erosion and less stable. This then leads to weakening the "sponge effect" of water storage. In the next stage of deforestation, the degraded forest holds less ecological value, but farmers increasingly see the

remaining trees as stored capital. The pine trees in particular, are often treated as a kind of savings account that can be harvested when cash is needed ([14]). The simplified, drier forest then becomes easier to clear for corn fields, and this ongoing process means that what remains of cloud forest is now largely confined to the steepest slopes and highest ridges, where access and cultivation are most difficult.

2.3. Hydrological Cycle and Fog Interception

The hydrological cycle is an ongoing process of water traveling between the atmosphere, Earth's surface and subsurface. Many processes are involved in this cycle, but in general water falls from cloud as precipitation. It then either (1) infiltrates the ground, (2) flows across the surface through the soil or bodies of water, or (3) evaporates. When water evaporates, it condenses to clouds, allowing water to constantly circulate between the sea, land, and air. A cloud forest adds another layer to this hydrological cycle, namely fog interception. This is illustrated in Image 2.8, with the fog interception being highlighted.

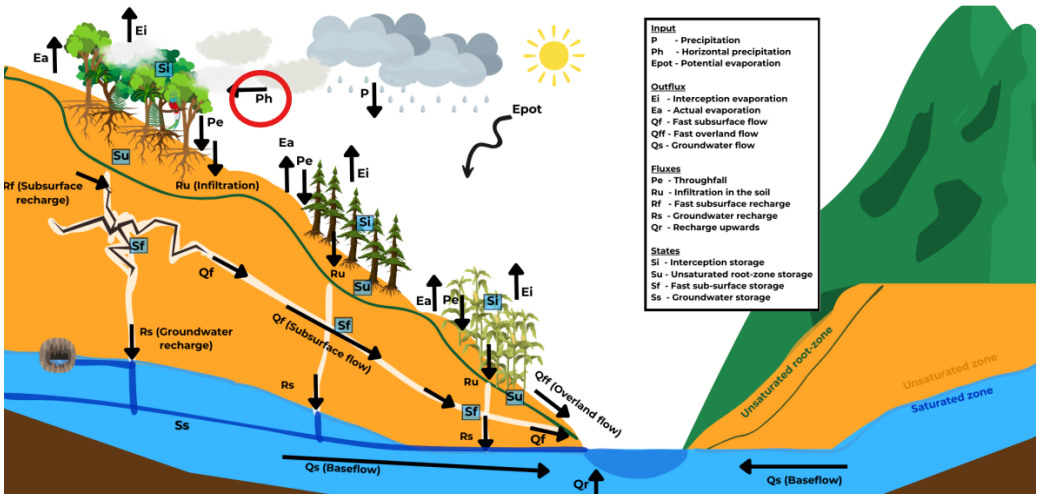

Figure 2.8.: Hydrological Cycle with Fog Interception ([13])

Fog interception is the process by which water droplets in the air (from fog or clouds) are captured by the forest canopy. The efficiency of fog interception is determined by three main factors ([24]). First, higher wind speeds increase fog interception since they lead to more droplet collisions ([3]). Second, topographic factors, such as being located within the cloud layer or closer to the coast, increase fog deposition. Finally, a denser cloud forest canopy increases the amount of fog interception ([24]). Depending on these factors, fog interception can contribute between 10% and 60% of the total moisture input to a system ([25]).

The cloud forest can also function as a hydrological buffer. Excess rainfall can get temporarily stored in the canopy, leading to a more gradual release of the water to the soil. At the same time part of the intercepted water can also evaporate, which increases the local humidity. Overall, this buffering effect helps to reduce the runoff peaks and stabilizes stream flow ([26]).

2.4. Change in Cloud Base Height

Fog interception plays an important role in the hydrological cycle of Alta Verapaz, where clouds forests rely on frequent low-lying clouds to capture additional moisture [13]. Changes in land use type could disrupt the system by altering the height of the cloud base. [27]. Warmer surface temperatures generate stronger convective uplift, pushing the clouds higher uphill. These warmer surface temperatures can be caused by a less dense canopy where the ground is less shielded from solar radiation. The air can also be cooled by vegetation as it gives the land an evaporative potential that uses solar energy for evaporation instead of warming the surrounding air. A loss in vegetation, like agricultural land, can therefore lower this potential and increase local air temperatures. At the same time, vegetation loss might reduce the humidity, as there is no/less evaporation. With lower humidity, the saturation of air with water vapor is less likely causing the clouds to form at higher altitudes. Figure 2.9 gives an illustration of the potential effects of land use change on cloud forest height.

2.4.1. Literature on Lifting Condensation Level (LCL)

Tropical montane cloud forests (TMCFs) depend on predictable, frequent, and prolonged immersion in clouds [10]. Cloud forests occur on mountain ranges that push winds up above the Lifted Condensation Level (LCL) causing clouds to form. The height at which this occurs is also known as the Cloud Base Height (CBH) which depends on how hot and dry the rising wind is.

Forests being immersed in cloud has several effects on the entire ecosystem. Most notable is that the forest is now able to directly access water from the atmosphere. Epiphytes thrive in cloud forest since they capture the water vapor particles from the clouds. This process is known as horizontal precipitation and contributes to the forest's hydrological cycle. This additional source of water is what allows biodiversity to thrive including many animals and fauna that cannot be found anywhere else [20]. Surrounding cities, villages or communities also often rely on water originating from cloud forests. Both because the horizontal precipitation provides a stable water supply and because it acts as a natural filtration system. Additionally the large potential of a cloud forest to hold water gives it a spunge-like function that allows for water release under dry conditions and a delay in water release under extreme wet conditions [28]. Moreover, clouds reduce incoming radiation and outgoing longwave radiation, increase humidity, and reduces transpiration. All of which impact the soil structure, nutrient cycling, and composition of the vegetation [10].

Up to 60% of moisture inputs into TMCFs can be attributed to cloud interception [3]. This is most significant during the dry season. But this resource is threatened by rising cloud base heights. Clouds are no longer sieving the forests at the same height, and sometimes missing the mountain entirely. In that case, the essential source of additional water is no longer present. There are several indicators of this. Studies using a ceilometer that measures the cloud base height directly with Li-DAR show a cloud base height increase of up to 300 meters [7], [29]. Regional atmospheric modeling also showed an increase in cloud-base height when considering climate change and deforestation [10]. Finally, there is also evidence of cloud reliant vegetation no longer being found at lower elevations but instead appears to be migrating upwards [30].

(a)

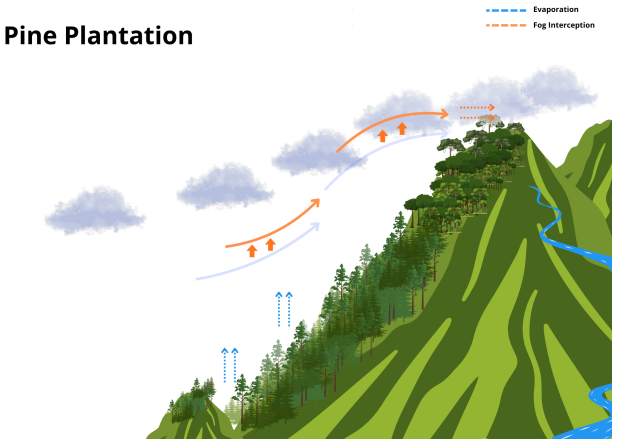

(b)

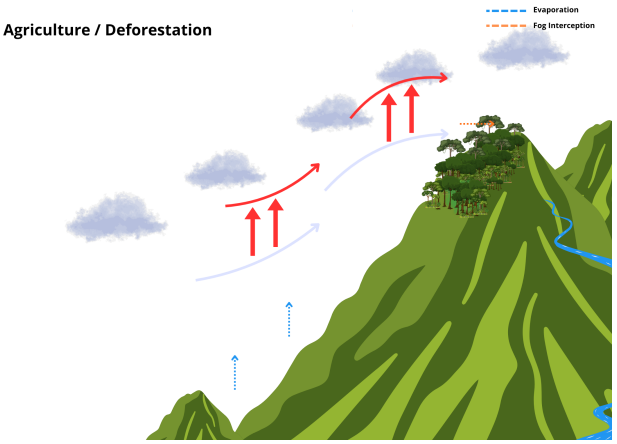

(c)

Figure 2.9.: Illustration of how land-cover type influences cloud formation and moisture dynamics along a montane slope. (a) Intact cloud forest enhances cloud interception and maintains cool, moist conditions.(b) Pine plantations alter airflow and reduce cloud-water capture efficiency compared to native forest.(c) Agricultural land and deforested slopes increase surface heating and upslope convection, reducing cloud immersion frequency and overall moisture retention.

Cloud-base height is rising for several reasons, including the effects of global warming. Higher surface temperatures increase the saturation specific humidity, and under the assumption of a constant adiabatic lapse rate this leads directly to a higher cloud-base height (CBH). This relationship is also reflected in the commonly used rule-of-thumb formula for cloud-base height. In her Cloud Chasers III project, [13] applied this approximation as proposed by [31].

$$z_{\text{CBH}} \approx 125(Tmp - T_d), \tag{2.1}$$

The other notable cause of changing cloud-base heights is deforestation. Deforestation changes atmospheric properties at a specific location. As explained before, cloud forests are extremely moist and relatively cool, with constant cloud cover and high humidity that support a rich diversity of epiphytes. When such a forest is cut down, the surface changes drastically. [10] States that "Reduced evapotranspiration after deforestation in tropical lowlands decreases the moisture content of the air mass flowing up the slopes of adjacent mountains. This increases the lifting condensation level and thus the elevation of the base of the cloud deck. The model results thus suggest that deforestation in the lowland tropics of the trade wind zone tends to shift the cloud forest environment upward in adjacent downwind mountains."

In this report a different method for calculating the cloud-base height was used. This method is explained more in depth in chapter 4.

2.5. Lifting Condensation Level Model

Lifting condensation level can be calculated using just temperature, humidity, and pressure measurements. The lifting condensation level is the height in the atmosphere at which an air parcel, when lifted adiabatically (without exchanging of energy, heat, with its surroundings), becomes saturated.

The maximum amount of water a parcel can hold is called the saturation vapor pressure (e_{sat}) which can be calculated by the formula [32]:

$$e_{\text{sat}} = e_0 \cdot \exp\left(\frac{b \cdot (T - 273.15)}{T - 35.86}\right) [Pa] \tag{2.2}$$

With $e_0 = 611.3$ and $b = 17.2694$.

The saturated water vapor specific humidity (q_{sat}) calculates the maximum amount of water vapor that the air can hold at a certain temperature before saturating [33].

$$q_{\text{sat}} = \frac{R_d \cdot e_{\text{sat}}}{R_d \cdot (p - e_{\text{sat}}) + R_d \cdot e_{\text{sat}}} \tag{2.3}$$

With $Rd = 287.05\ J/kg/K$ dry air gas constant ; p_{surface} = 85000 Pa.

The model finds the LCL by intersecting the specific humidity q_v with the saturated specific humidity e_{sat}, that is dependent on height as it is calculated with a temperature profile. The relative humidity is based on the relationship between vapor pressure and saturated vapor pressure x 100%.

Mixing ratio r and specific humidity q_v [32]:

$$r = \frac{\varepsilon \cdot e}{P - e} \quad , \quad \varepsilon = \frac{R_d}{R_v} \tag{2.4}$$

$$q_v = \frac{r}{1 + r} \tag{2.5}$$

Calculating the temperature of an air parcel based on height from the surface and the surface temperature.

$$T_{\text{profile}}(z) = T_{0k} + \gamma_T \cdot z \tag{2.6}$$

$$\gamma_T \equiv \frac{\Delta T}{\Delta z} = \frac{-g}{c_p} = -9.8/1000[K \cdot m^{-}1] \tag{2.7}$$

With T_{0k} being surface temperature (z=0).

Temperature, relative humidity, and pressure data generate T_0, e, e_sat, and p_{surface}. A python script was developed to calculate the cloud base height based on these formulas.

Note that temperature and humidity are the key determinants of cloud-base height in this model, but they are not the only relevant variables. A more precise assessment would require additional variables, such as atmospheric stability, turbulence, boundary-layer dynamics, orographic forcing, and several others. However, developing a full model for cloud-base height is beyond the scope of this project. Instead, we focus on the two most influential factors in this process and use the observable differences in these variables to provide an indication of their potential impacts on cloud-base height.

Cloud forests are characterized by horizontal precipitation, which is essentially intercepted fog due to passing low clouds. To study and quantify the hydrologic cycle and its effect on the Mestelá river, it is important to know where the base of the clouds are and if they can be intercepted by the forest. The elevation in cloud base height and therefore a reduced water yield might be significant for local communities, mainly during the dry season [34]. In the rainy season, when water is abundant, fog interception is a small fraction of the total available water. In those months, it is not the scarcity of water that causes problems but the characteristics of the deforested land. The increased run off due to deforestation can cause floodings. Although the atmospheric effects of deforestation on cloud base height may be more severe in the dry season, the data of this project, collected during the first weeks of the rainy season (sep-oct), can be extrapolated to other seasons and give a good overview of the influence of land use change.

2.6. Socioeconomic Relevance of the Study Area

Alta Verapaz is among the poorest regions in Guatemala, yet simultaneously constitutes a tropical biodiversity hotspot. This combination of high ecological value and widespread socioeconomic vulnerability creates a complex development context in which environmental degradation and human wellbeing are deeply intertwined [35]. Current agricultural practices, particularly forest conversion and land intensification, threaten both ecosystem integrity and long-term livelihood sustainability, making the region highly relevant for integrated environmental and socio-hydrological research.

2.6.1. Education, Livelihood Strategies, and Cultural Embeddedness

Education plays a critical role in shaping livelihood outcomes in rural Alta Verapaz. Interviews conducted during fieldwork and discussions with local engineers and CCFC staff indicate that household-level education, particularly when at least one child participates in formal schooling, can significantly influence decision-making processes related to farming and nutrition. Knowledge introduced by younger household members often carries social legitimacy within families and facilitates change more effectively than external interventions.

Maize cultivation remains culturally ingrained in daily life and identity, commonly expressed through the local notion that "corn is life" [22]. Despite its central symbolic value, maize production is economically inefficient under current market conditions, as local farmers often sustain higher production costs than the price at which maize can be purchased. According to CCFC representatives, this paradoxically perpetuates poverty rather than alleviating it. Similar patterns are documented in [35], who identified maize and beans as the dominant subsistence crops in the region, despite their limited income-generating capacity.

In response to declining profitability of traditional crops, many households have transitioned into alternative land uses such as pine forestry or contract farming agreements for export-oriented crops including avocado and carrots. However, these alternatives frequently involve dependence on external buyers, exposure to price exploitation, and intensive pesticide application, introducing new ecological and health risks. This shift away from diversified agroforestry toward monoculture production undermines resilience and reinforces economic vulnerability.

2.6.2. Agroforestry Systems and Their Development Potential

The capacity of agroforestry systems to support both environmental and socioeconomic outcomes is well documented, including improvements in income diversification, resilience to climate variability, and sustainable natural resource management[36]. In Alta Verapaz, however, widespread land-use practices such as slash-and-burn cultivation continue to dominate and pose a serious threat to forest ecosystems [35].

Between 2006 and 2010, Guatemala lost an average of 132,137 hectares of natural forest per year, making it the country with the highest deforestation rate in Central America [37]. While forest conversion is commonly justified by the need to meet rising food demand, this

approach is not sustainable in the long term and leads to soil degradation, biodiversity loss, and hydrological disruption [38].

Nicli reports that Alta Verapaz is home to approximately 1.25 million inhabitants and is one of Guatemala's most densely populated departments, with an average of 145 inhabitants per km². Roughly 80% of the population resides in rural areas, and around 90% identify as indigenous Q'eqchi' or Poqomchi' Maya [**?**]. Food insecurity is widespread, with moderate to severe food insecurity affecting approximately 55% of households [35].

The region's cropping systems are diverse but heavily dominated by low-value or environmentally intensive crops. Major productions include maize, beans, coffee, chili pepper, cocoa, vanilla, cardamom, and a variety of fruits and timber species. These systems often operate under conditions of small landholdings: [35] found that the mean landholding size among agroforestry farmers was only 3.5 ha (SD = 2.6 ha), with an average household size of 6.7 members. The surveyed farmers were all male specialists with a mean age of 49.6 years, highlighting gendered access to land and decision-making structures within agricultural systems .

2.6.3. Water Scarcity and Infrastructure Failure

Hydrological stress is increasingly evident across Alta Verapaz. Community interviews highlight declining dry-season water availability combined with rising frequency of extreme rainfall events. In 2018, Cobán experienced severe drought conditions that significantly reduced both water quantity and quality. Several surrounding villages reported receiving water supplies only three days per week, and residents reported visible declines in water clarity.

Despite the presence of five treatment plants in Cobán, none are currently operational due to financial constraints. The result is widespread dependence on untreated surface water, heightening health vulnerability. Field interviews further indicated an increase in gastrointestinal diseases and potential links between agricultural contamination and public health outcomes (Rob Cahill, personal communication, 3 September 2025).

2.6.4. Land Conflict, Environmental Degradation, and Structural Inequality

Land constitutes both material wealth and cultural identity in Alta Verapaz. Population growth, estimated at approximately 1.5% annually [35], intensifies competition for arable land and accelerates deforestation. Informal land transactions further aggravate this situation; reports indicate that vulnerable families are sometimes sold land without proper legal ownership, leading to conflict and displacement.

Commercial agriculture has also expanded rapidly, particularly avocado plantations driven by external investment. Adjacent plantations were observed to apply heavy pesticide loads and construct artificial drainage channels, which increase runoff, sediment transport, and chemical influx into local river systems. Farmers and health workers reported concerns about rising stomach cancer incidence following expansion of agrochemical-intensive farming, though causal linkages require further investigation.

At the structural level, Guatemala exhibits severe wealth inequality. Approximately the bottom 50% of the population controls only 3.5% of national wealth, while the top 10% holds 64% [39]. These disparities severely restrict access to education, health services, legal protection, and economic mobility for rural populations [40].

2.6.5. Relevance for This Project

The socioeconomic conditions of Alta Verapaz underscore the necessity of integrating hydrological modeling with social analysis. Fog interception, water availability, and land-use change are not abstract processes but directly shape nutrition, public health, income stability, and ecosystem resilience. By combining environmental monitoring with community insights and livelihood analysis, this project contributes to understanding both the biophysical and human dimensions of sustainability.

In this context, the project does not merely seek ecological insight but aims to provide scientific support for livelihood transitions toward sustainable agroforestry systems that reconcile conservation objectives with human development needs.

3. Materials and Set-up

In this chapter, all materials and methods to gather sufficient and reliable data are discussed. A variety of different tools and materials are needed.

3.1. Measuring devices: LogTags and Divers

In this project, 2 different measuring devices are mainly used: LogTags and Divers. Both of these devices are discussed in this section. Additionally, the measuring devices installed on the tower constructed by the Cloud Chasers IV project are also used as input data.

3.1.1. LogTags

This study uses data loggers (*LogTags*) to measure air temperature and humidity, to obtain a vertical profile of temperature and humidity from ground level to the canopy of the cloud-forest. Before field deployment, a series of tests was performed in order to (1) validate the devices against a reference instrument, (2) determine the optimal setup and (3) evaluate placement effects by installing units at multiple locations, so that potential environmental influences can be anticipated.

The front and back of the logtags can be seen in 3.1b and 3.1a. These are built to perform in outside environments and can measure. LogTags (HAXO-8 models) are compact humidity-and-temperature data loggers that measure up to 8,000 paired readings over a wide range (-40 °C to 85 °C, 0–100 percent RH). It includes a real-time clock that time-stamps every measurement and a small, durable case, making it suitable for tracking environmental conditions continuously.

To find the optimal configuration of the LogTags, responses to altitude, the sensor height above the ground and logging interval were examined. For the configuration of the LogTag, interval time is most important. Figure 3.2 shows series A (2 min) and E (10 min).

As can be seen in Figure 3.2, the 2-min (A) and 10-min (E) series track the same overall pattern, but the coarser interval smooths out the short time short fluctuations. In this fast changing environment, these local extrema matter. Peak and trough counts tell the loss of detail at 10 minutes. For temperature, A registers 36 peaks and 37 troughs versus 17 and 16 for E (Δpeaks = 19; Δtroughs = 21). For relative humidity, A shows 53 peaks and 52 troughs versus 12 and 12 for E (Δpeaks = 41; Δtroughs = 40). Although the broader trend is preserved, the 10-min interval misses many local maxima and minima. Given that the LogTag memory can support a 2-min interval over a 7-day deployment, the 2-min setting is adopted for future measurements.

(a) Back of LogTag labeled B

(b) Front of LogTag

Figure 3.1.: Back and front view of the LogTag

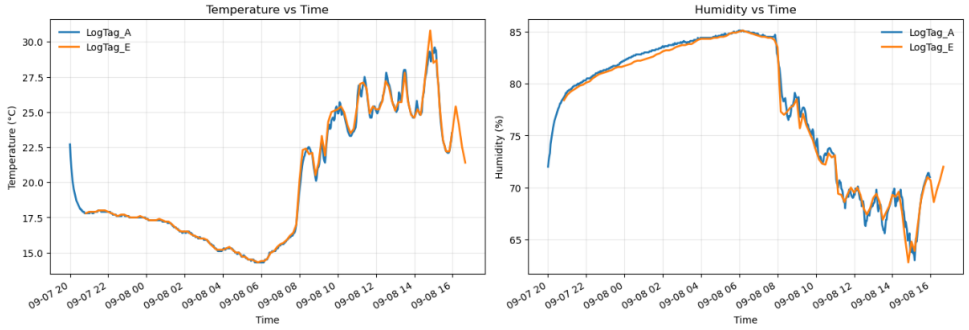

Figure 3.2.: LogTag interval comparrison 2min vs 10min

3.1.2. Divers

The TD-divers in this project, are primarily used to measure atmospheric pressure, which influences the Cloud Base Height that will be determined later in this project. The sensors of the 3 divers used, record both pressure and temperature with a very high precision. The temperature sensor has an accuracy of ± 0.1 °C ([41]), making it suitable for validating the temperature readings from the LogTag sensors, which is a more simple measuring device. The interval time for the diver data is 2 minutes, the same as for the LogTag readings.

The TD-Divers are deployed together with the LogTag that is just above ground surface level.

Each diver is placed in a handmade protective case, to prevent it from exposure to rain, dirt and impacts. Figure 3.3 is added as a visual representation.

(a) TD-Diver ([41]) (b) Protective case (c) Deployment

Figure 3.3.: Diver, protective case & deployment of diver

3.1.3. The tower (Cloud Chasers IV)

The previous Cloud Chasers group, constructed a 13.5 meter, in-canopy tower. On top of this tower, multiple measuring devices were installed, such as a tipping-bucket rain gauge (for vertical precipitation), fog traps (for horizontal precipitation), a wind speed sensor, a temperature and relative humidity sensor and a solar radiation sensors. All instruments are connected to a data logger that records and stores the measurements. At a later stage, the data can be used as input for the hydrological model [42]. The tower is shown in Image 3.4.

3.2. Pulley System

To obtain the vertical profile mentioned in the LogTag section, the LogTags must be placed in the canopy. A fishing line is first launched over a tree branch using a bow and arrow. This line is then attached to the pulley cord and used to pull the pulley over the branch. When tensioned, the system sits firmly around the branch, allowing the instruments to be raised and lowered. An additional loose hanging eye on the system allows the retrieval from the canopy. By pulling on the eye, with a hook attached on the pulley rope, the whole setup can be lowered and removed, ensuring that no materials are left in the cloudforest. As a visual interpretation of the system, the pictures in Figure 3.5 have been added.

Figure 3.4.: Bottom & side view tower [42]

(a) Pulley system (b) Bow and arrow (c) System up a tree

Figure 3.5.: Pulley system procedure

3.3. Radiation shields

Incoming solar radiation can heat sensors and cause overestimation of air temperature. Radiation shields are therefore required that block direct radiation while allowing sufficient airflow for reliable measurements. Based on preliminary research into low-cost radiation shields, several shield designs were tested.

3.3.1. Preliminary research

Preliminary research indicates that passively aerated, cost-effective radiation shields can achieve accuracy within 0.5 °C, which is comparable to more expensive commercial designs ([43]). The designs generally use a layered configuration with 20–30 mm spacing between plates. Aluminum foil is used as the primary material, because it has a reflectivity up to 0.9. When applied to the outer surface of the top plate, it reflects most incoming solar radiation and therefore strongly reduces radiative heating. It also helps limit both longwave and reflected shortwave radiation reaching the sensor ([44]). The shields typically use bowl-like geometries with flat bottoms or curved rims that admit airflow for passive ventilation while still shielding the sensors.

Besides solar loading, albedo, and material properties, there are also concerns about wind speed introduction an error aerodynamic heating of the sensor. This effect increases with wind speed, however is negligible below roughly 20–30 m/s ([44]). In the present cloud forest setting, the average wind speed during September was below 2.5 m/s according to the local weather station, so aerodynamic heating is considered negligible. Although the plates of the shield may increase air movement around the sensors, the induced flow is not expected to exceed about 1.113 m/s, as found by reported values in studies ([44]).

3.3.2. Designs

The preliminary research explained in the previous paragraph is used as a kickstart for the desing of radiation shields. At the same time, the designs were not solely fixated on the published results. A range of alternative configurations was developed and empirically tested.

Figure 3.6 shows the range of radiation shields tested. These radiation shields are tested by comparing the LogTags that are in a radiation shield, to a base LogTag for both the temperature and humidity measurements. In Figure 3.7 the results of this first day of testing are shown. In Appendix A there is a clear overview of all the radiation shields that have been tested, with a short description and an image.

After reviewing the first-batch results, it became clear that the temperature record of the control LogTag was corrupted (the thicker line). Now, selecting the most effective radiation shields relied on identifying the LogTags that recorded the lowest temperature, which can be interpreted as better shielding and better airflow guidance. The humidity records were good, allowing straightforward selection based on those results. A second round of tests was therefore conducted using the Diver as the temperature reference instrument. The outcomes are shown in Figure 3.8.

Following the second round of testing, Big Collin performed best when compared to both the baseline LogTag for humidity and the Diver for temperature. This is likely because it has the best design against radiation, while also keeping sufficient airgaps to remain airflow. The design is shown in Figure 3.9. While its temperature record closely tracked the baseline (the Dome), the humidity response left room for improvement. Accordingly, the design was refined to increase airflow: an updated version using the inverted cake pans is created to

Figure 3.6.: Range of radiation shields of first batch

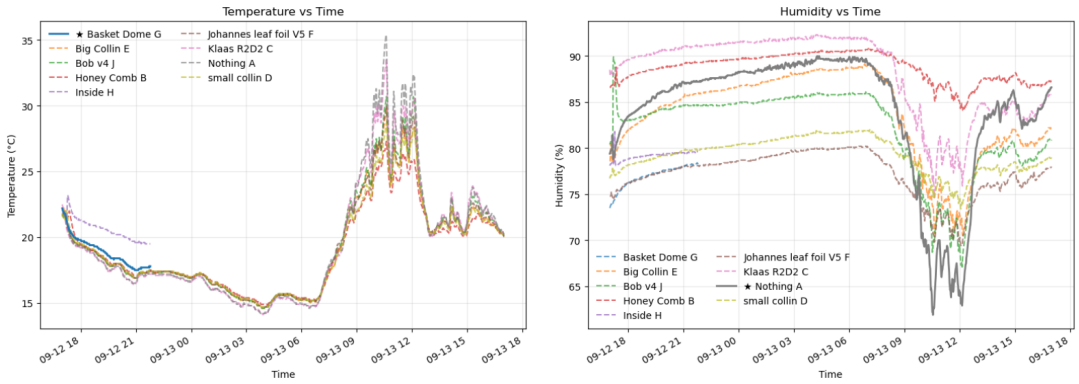

Figure 3.7.: Results radiation shield testing 1

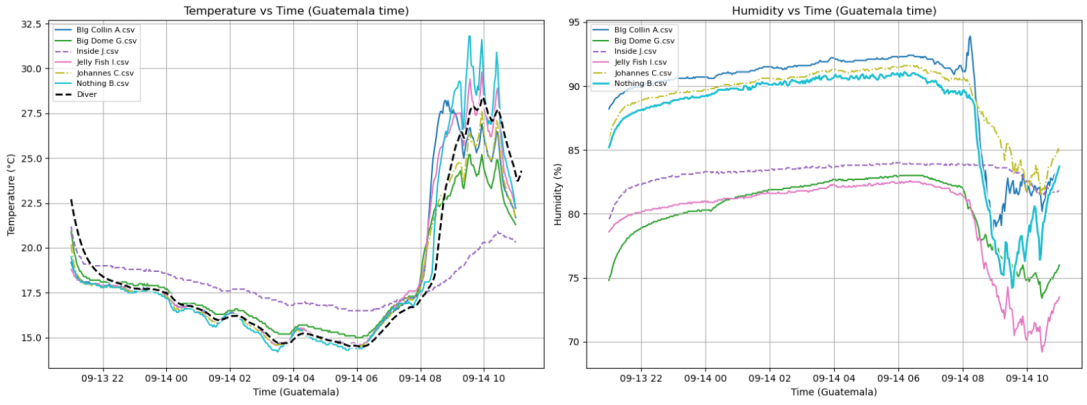

Figure 3.8.: Results Radiation Shield Testing 2

increase the airflow more effectively. This design is in line with insights from the preliminary literature. Additional vent holes were added to the top plate. The revised, three-layer design is shown in Figure 3.10.

Figure 3.9.: Big Collin

Figure 3.10.: 3 layer radiation shield

3.4. Camera

In addition to the measurements from the LogTags, a camera system is used to visually detect cloud presence. The camera serves to provide visual confirmation of the LogTag records and also to enable qualitative comparisons based on imagery. For example, to confirm if there are differences between pine forest and cloud forest.

Preliminary tests with the camera indicated that a two-minute interval is suitable. At a five-minute interval, changes in cloud formation were already missed, as clouds form and disappear rapidly in this watershed. The camera was positioned to view the LogTag site from a greater distance. An example of both the camera output and the camera placement is shown in Figure 3.11.

3.5. Research locations

Data were collected in three vegetation types: cloud forest, pine forest, and deforested areas. These sites are selected for several reasons. The cloud forest represents the natural vegetation of the catchment. Second, pine forest is of interest because it is widespread in the region. It is promoted by Guatemala's Ministry of Forestry for its higher economic returns compared to cloud forest, which has led to the conversion of cloud forest into pine plantations. Finally, deforested areas are included to represent common land uses, such as cattle

(a) Example camera output

(b) Example camera placing

Figure 3.11.: Example of the camera setup and corresponding output

land and cornfields.

Data will be collected in five rounds. Each round lasts approximately seven days, after which the LogTags are relocated to new positions. Further details on the locations are provided in the following paragraphs. The rough locations of the 5 batches are given in Figure 3.12.

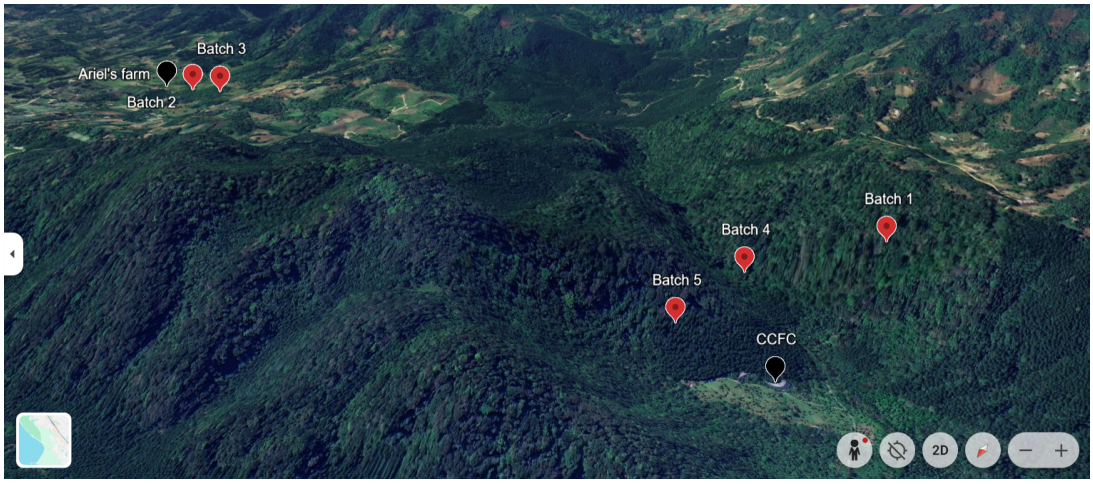

Figure 3.12.: Locations of all the batches

3.5.1. Cloud and Pine Forests: Comparison by Altitude (Batch 1)

In the first round, the comparison between cloud forest and pine forest has been made, with emphasis on altitude effects. A cloud-forest site and a pine-forest site were selected at ,1,665 m a.s.l., and an additional site at 1,555,m a.s.l. All sites were placed on simliar slopes to

limit differences due to topography. Equipment installed at the upper cloud-forest site was stolen, so the site was moved to another ridge near CCFC, at roughly the same altitude as the original site. The locations of these sites are given in Figure 3.13. Images of the specific tree's on the sites are given in Appendix B.1.

Figure 3.13.: LogTag locations of Batch 1

3.5.2. Ariel's Farm: Agriculture, Pine Forest & Native Forest (Batch 2)

The second round of measurements takes place on the land of a cattle farmer (Ariel's farm). The property contains all three site types of interest, namely agricultural fields, a pine plantation, and native forest with scattered pines, which makes it suitable for comparison. Conducting the tests on a single, privately managed property also reduces the risk of theft of the equipment. For this data collection round, two testing sites were established on agricultural land, two in the pine forest and one in the native forest. The locations of these sites are given in Figure 3.14. Images of the sites in reality and a more detailed description are given in Appendix B.2.

3.5.3. Ariel's Farm revisited: simplified setup (Batch 3)

The third location is once again Ariel's Farm, as the site proved particularly suitable for the investigation. The primary purpose of this batch was to collect additional data from this location. Some LogTags were removed to make them available for deployment at other sites. In Batch 2, two trees per location were used to validate the data; after this validation was completed, repeating the same setup was considered unnecessary. The full setup in Ariel's Farm now consists of 1 tree in the Native Forest, 1 tree in the Pine Forest and 1 tree at the Agricultural Field, all with only 2 LogTags. A more detailed description is given in Appendix B.3

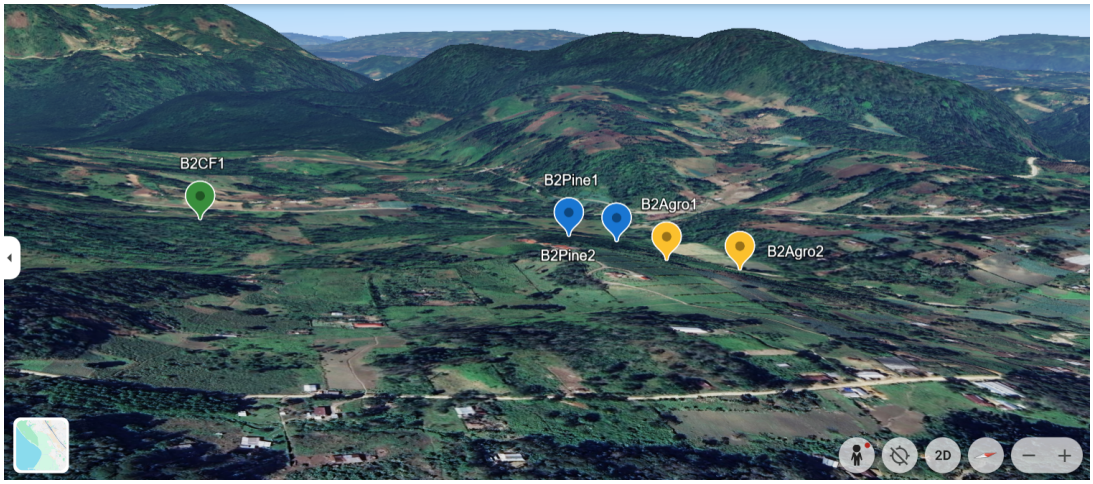

Figure 3.14.: LogTag locations of Batch 2

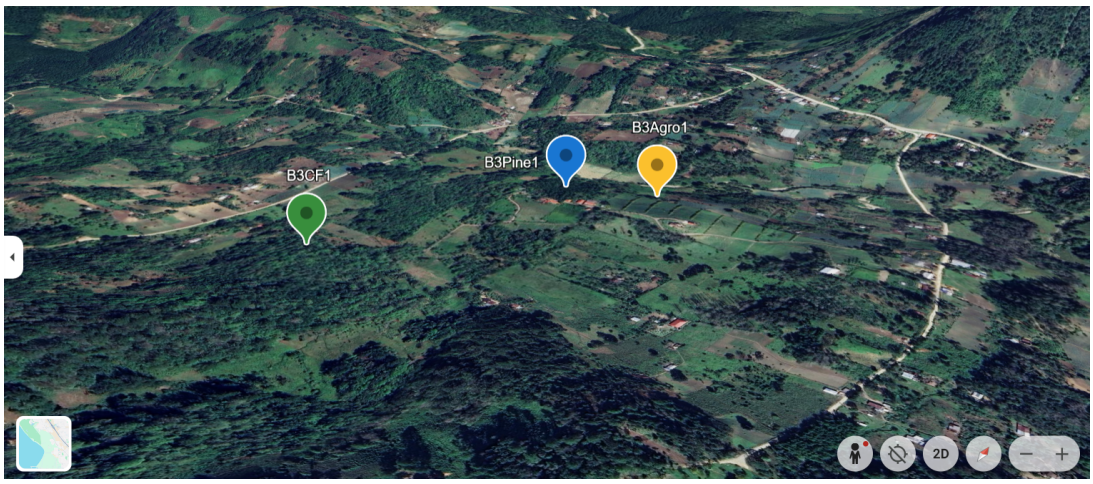

Figure 3.15.: LogTag locations of Batch 3

3.5.4. CCFC 1: Cloud Forest, Pine Forest & Open Field (Batch 4)

The fourth batch was conducted around CCFC to take a closer look at the area from which the project operates. This location has a very variable climate with different types of vegetation. Another advantage of this site is that the risk of equipment being stolen is very low, since all sensors are placed within CCFC property.

In this batch, comparisons were made between the Cloud Forest, Pine Forest, and Open Field. Within the Cloud Forest, an additional comparison was made between a more open and a denser area. The locations of the deployed LogTags are shown in Image 3.16, and a more detailed description is provided in Appendix B.4.

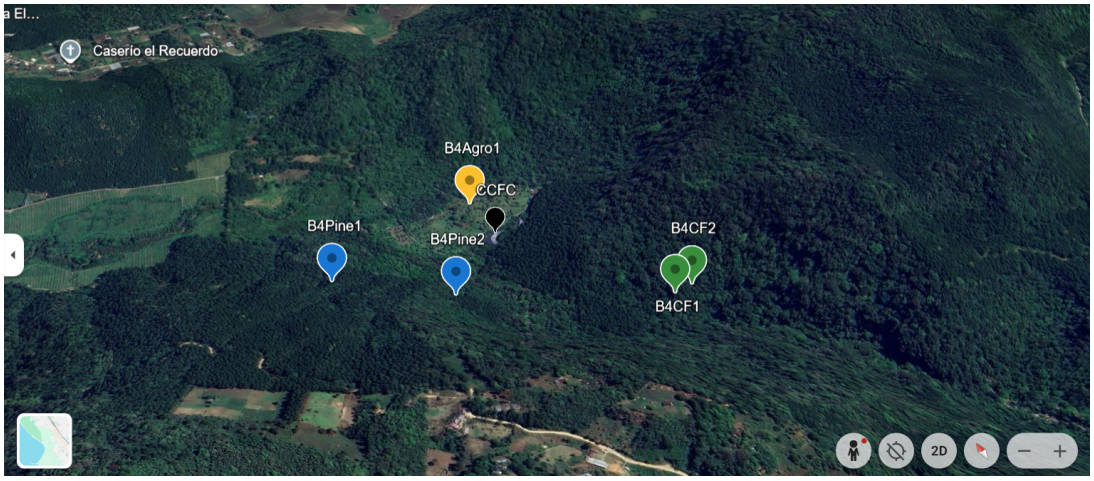

Figure 3.16.: LogTag locations of Batch 4

3.5.5. CCFC 2: Collecting Additional Data (Batch 5)

The fifth and final batch focused on collecting as much data as possible. For this batch, additional measurements were taken at two Cloud Forest locations and one Pine Forest location, all located around CCFC. The focus on Cloud Forest sites was chosen because fewer of these had been measured previously. The locations at Ariel's Farm were considered more like Native Forest because the Cloud Forest is characterized by greater variability, more data is required to draw reliable conclusions. A more detailed description of the site is provided in B.5. The locations are given in Image 3.17.

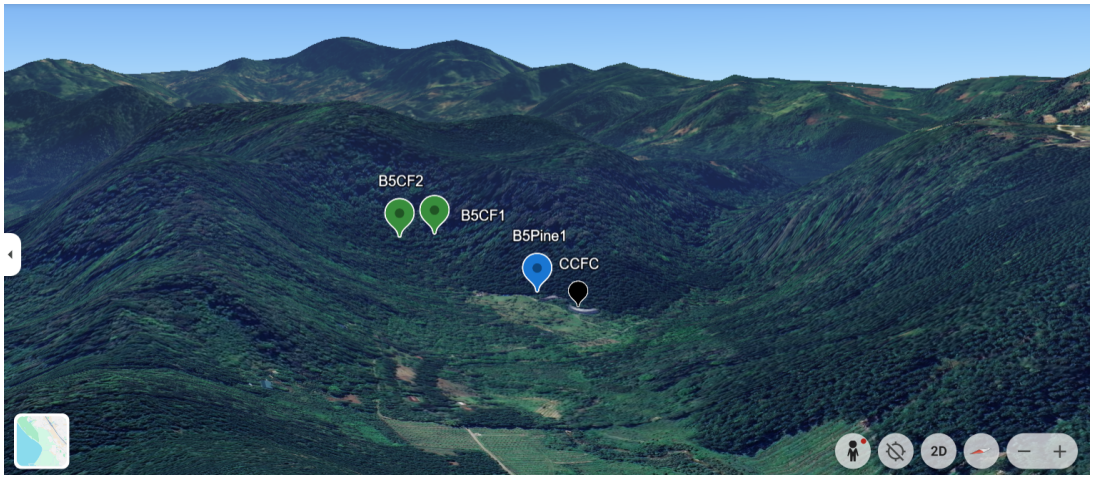

Figure 3.17.: LogTag locations Batch 5

4. Methods: Cloud Base Height

The first outcome this project aims to study is the difference in CBH in the different types of land use. As explained before and illustrated in Figure 2.9, it is hypothesized that CBH would be lower for cloud forests than for pine forests and a pine forest would have a lower CBH than agricultural, low crop lands. The height of clouds affects the forest's water cycles, that consequently affect river flow and discharge - therefore influencing all the surrounding communities that depend on this river water for everyday life.

4.1. Comparison of CBH of different Land Use Types

To estimate cloud-base height for the different land-use types, temperature and humidity data recorded by the LogTag sensors were used to calculate the lifting condensation level. Measurements were carried out at two main locations: Ariel's farm and the area around the CCFC campus.

Ariel's farm, located close to the CCFC campus, offered access to three different land-use types in close proximity. Data collection took place during two separate one-week campaigns. In the first week, a larger number of LogTags were deployed with two measurement points assigned to each land-use type. After this initial period, some sensors were removed, but a smaller group remained in place to continue the observations. It should be noted that a true cloud forest was not available at this site. Instead, measurements classified here as "mixed forest" were taken in an area containing native species, deciduous trees, a few cloud-forest species, and all mixed with some pine trees. Even so, this mixed-forest area was expected to show different conditions compared with the pine forest and the agricultural (grassland) site.

Around the CCFC area, measurements were taken for approximately one week in cloud forests, pine forests, and an open field used for agroecological activities.

4.1.1. Temperature profiles of different Land Use Types

In this research, the air temperatures of different land-use types were measured due to air temperature being a component of great importance to the LCL model. Multiple modeling and observational studies have show the relationship between deforestation and warming [7], [8], [9] and the effect on the LCL [7], [10]. The estimated influence of land cover differences on cloud base height is based on the relationship between air temperature and dew point temperature. This relationship is closely linked to the surface, as the physical characteristics of a surface influence how energy is absorbed, stored, and released into the surroundings. These physical characteristics can, for example, determine the albedo, the heat storage capacity, or the amount of evapotranspiration of the surface. The way incoming energy fluxes are partitioned at the surface determines, among other things, the warming of

the air. Since warmer air can hold more water vapor, this also influences the height at which air gets saturated and clouds start to form.

Based on the differences observed in the land characteristics of cloud forests, pine forests, and agricultural land, it can be expected that these translate into differences in energy partitioning. Albedo, for example, is lower in forested areas and results in less reflected radiation. On the other hand, open areas have a lower thermal mass and heat up quicker because they store little energy internally, causing the air temperature to rise quickly too. Another factor is (evapo)transpiration which is a strong driver to cool the air temperature as vegetation absorbs incoming solar radiation energy, but instead of converting it into sensible heat that warms the surrounding air, much of this energy is used to drive the phase change of water from liquid to vapor. In this, vegetation type is very important and mainly cloud forests, with more dense humid vegetation compared to pine, drive strong evapotranspiration.

These are just a few factors that indicate the air temperatures at surface level, while the complete system is far more complex; this includes, for example, local weather, wind, elevation, topography, slope orientation, and many more. In this study, the studied areas are at close proximity to each other and measured in overlapping time spans, which cancels out some of these factors. Therefore, it is clearer to assign differences in air temperature to varying types of land use. The air temperatures at Ariel's farm and CCFC are shown in 4.1 while 4.4 and 4.5 show the mean temperatures.

Figure 4.4 shows the mean daytime and nighttime temperatures (in degrees Celsius) of mixed forest (native species mixed with pine), pine forest and open field (open agroforestry parcel) at the Ariel's farm location. The daytime data is from 06:00 to 18:00, and nighttime from 18:00 to 06:00. It is clearly represented that mean nighttime temperatures are very similar for each type of land measured. This highlights the importance of the diurnal cycle on temperature changes, as well as justifying not having a focus on nighttime measurements for deeper data analysis.

Daytime measurements show higher mean temperatures for the Open Field location. This is likely due to radiation being able to access the surface without any obstruction on its path. This translates into direct radiation heating the ground and consequently warming the air. Mixed forest and pine forest have closer measured values for the temperature averages, highlighting the role of the canopy and vegetation underneath it and closer to the surface.

Figure 4.3 shows the results of CCFC and 4.2 shows the results of Ariel's Farm. The figure shows differences, mainly during the day, with average daytime differences in the cloud forest being 1.1 degrees Celsius cooler than the pine forest and 1.8 degrees Celsius cooler than in the open field. These lower temperatures in the cloud forest can be explained by the dense vegetation that has strong abilities to use incoming solar radiation energy for evapotranspiration. Standard deviations indicate that daytime temperature fluctuations were greater in the open field, consistent with the lower thermal mass of grass and bare soil compared to forested sites, which allows air temperatures to change more rapidly.

The following figures show the mean temperatures during the daytime (06:00 - 18:00) for Ariel's farm and CCFC campus of all LogTags averaged together and classified by land-use type. Clearly shown in the graphs, open field measurements have a higher average. It is interesting to highlight that the mean temperature between for Mixed and Pine forests is the same in the location of Ariel's farm, with a bigger standard deviation for Mixed Forest. In CCFC, these show differently: Cloud Forest's mean temperature is visibly lower than that of Pine forest, confirming the expectations for this first round of measurement results.

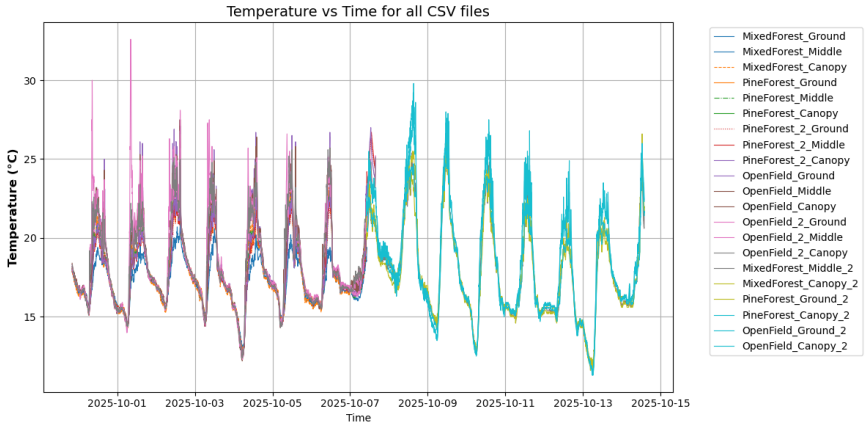

(a)

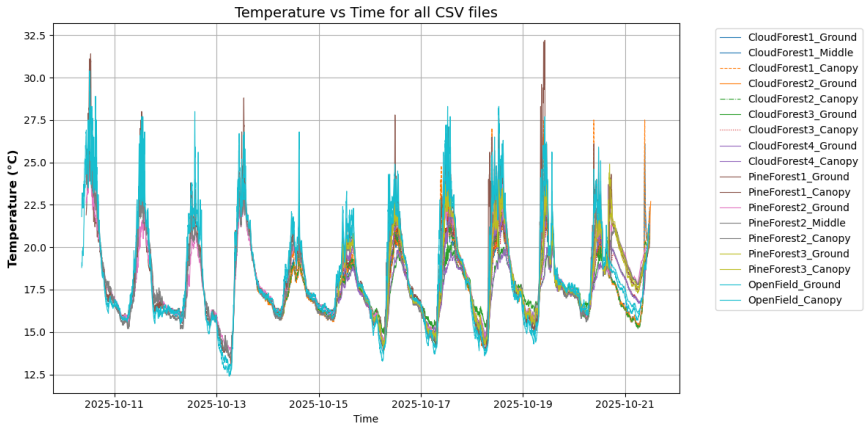

(b)

Figure 4.1.: Temperature profiles of different LogTag sensors during the measured time at Ariel's farm (a) and CCFC (b).

4.1.2. Humidity profiles of different Land Use Types

Humidity plays a key role in determining the lifting condensation level. An air parcel can contain only a certain amount of water vapor before it saturates and condensation start. The LCL represents the height at which an ascending air parcel reaches this saturation point. Because saturation vapor pressure increases with temperature, warmer air can hold more water vapor before condensation occurs. The previously discussed temperature results therefore suggests that warmer land-use types, like agriculture or pine, may produce higher LCLs, as the air above them can hold more moisture before saturating.

However, the LCL depends not only on the temperature but also on the relative humidity. That is the actual vapor pressure compared to the maximum vapor pressure at that temperature. Surface properties can influence this relative humidity. Air above sea generally has a higher relative humidity compared to the air over land due to the greater potential for evaporation. As an air parcel rises, it cools, lowering its water-holding capacity until

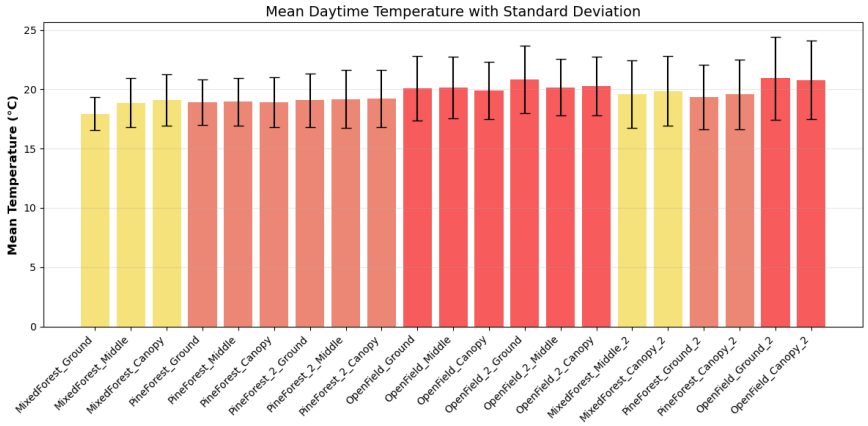

(a)

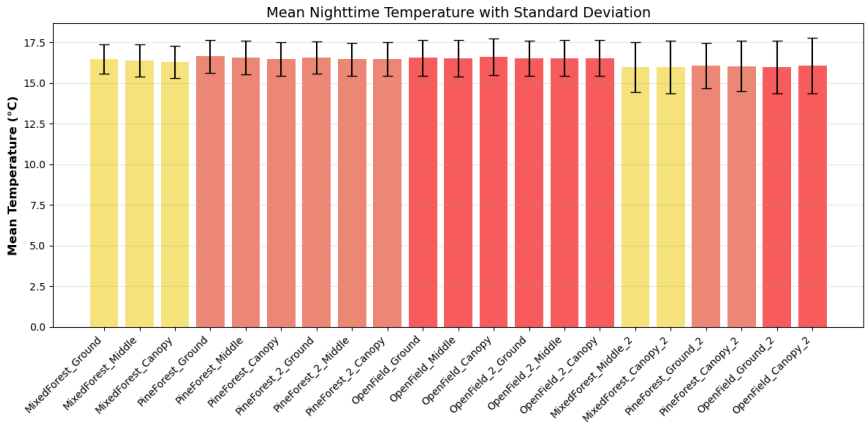

(b)

Figure 4.2.: Ariel's Farm: Mean daytime (a) and nighttime (b) temperatures for each sampled location at Ariel's farm site, with error bars representing ±1 standard deviation. The figure illustrates diurnal temperature variability and site-to-site differences in thermal behavior.

it reaches the condensation level. When the relative humidity or the absolute humidity is higher than this air parcel, clouds form at lower altitudes.

Figure 4.6 shows the relative humidity of the studied surfaces. As in the previous temperature figure, measurements are separated into daytime (a) and nighttime (b) intervals, measurements were taken at different heights within the tree canopy. The graph also shows nighttime relative humidity measures of near or exactly 100. These numbers represent the clouds forming at night due to the low temperatures (lack of incoming shortwave radiation), and the air saturating due to the high amounts of humidity.

At Ariel's farm, Figure 4.7, the humidity levels at night show the condensation (cloud formation). During the daytime, the lowest humidity averages are those taken in the Open Field measurements. The expected outcome was to have higher humidity levels in the mixed forest, due to the diversity and multitude of vegetation species. However, the graph shows some sensors that measure up to 10% less relative humidity than those of the Pine Forest.

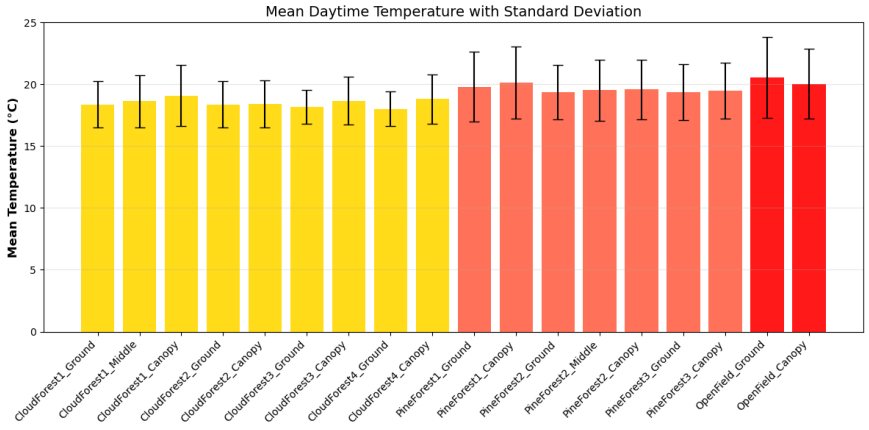

(a)

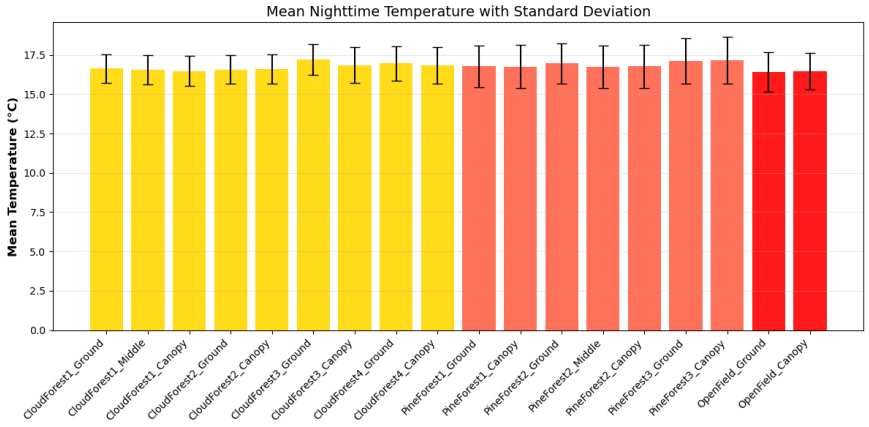

(b)

Figure 4.3.: CCFC: Mean daytime (a) and nighttime (b) temperatures for each sampled site, with error bars representing ±1 standard deviation. The figure illustrates diurnal temperature variability and site-to-site differences in thermal behavior.

This will show an impact on the height of LCL for each land-use type.

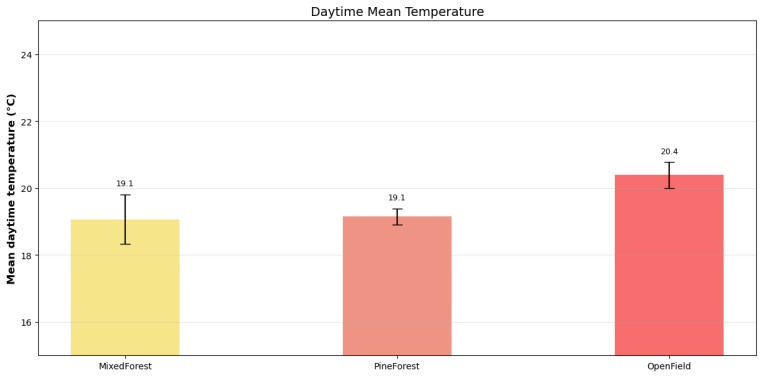

Figure 4.4.: Average temperature for the daytime at Ariel's farm.

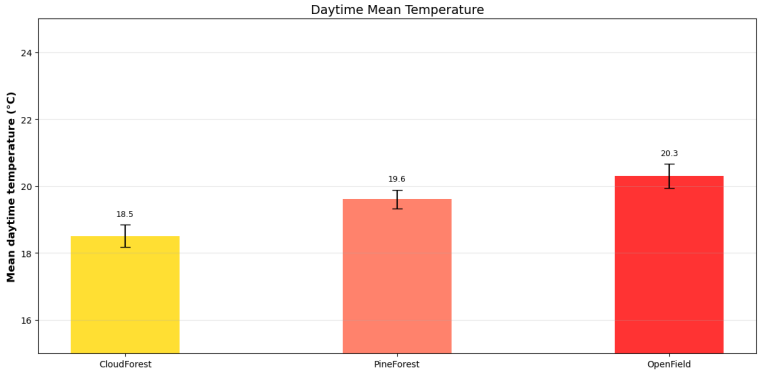

Figure 4.5.: Average temperature for the daytime at CCFC.

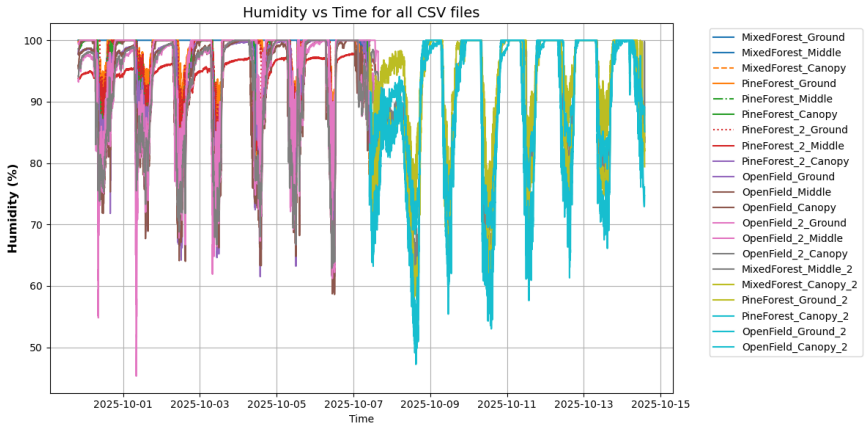

(a)

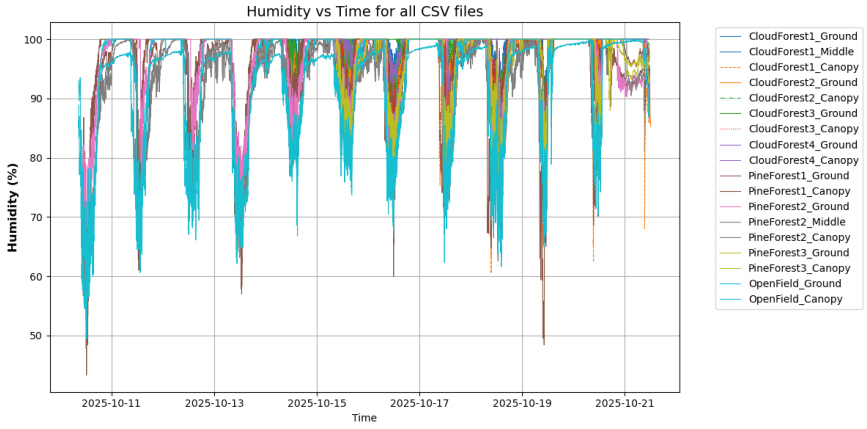

(b)

Figure 4.6.: Relative Humidity profiles of different LogTag sensors during the measured time at Ariel's farm (a) and CCFC (b).

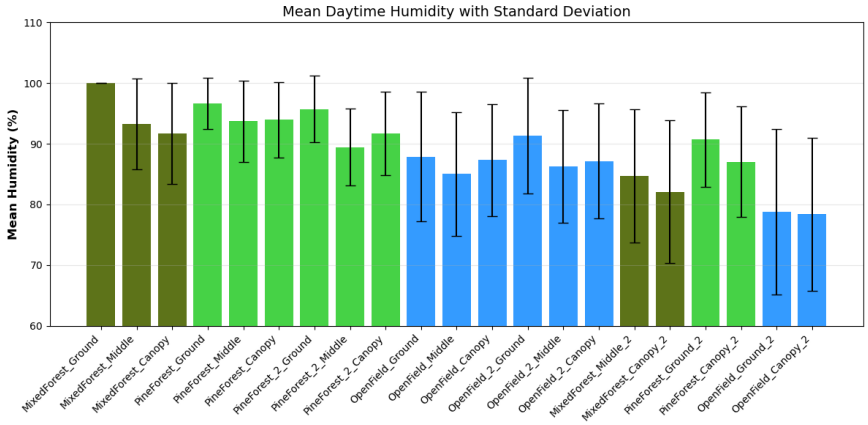

(a)

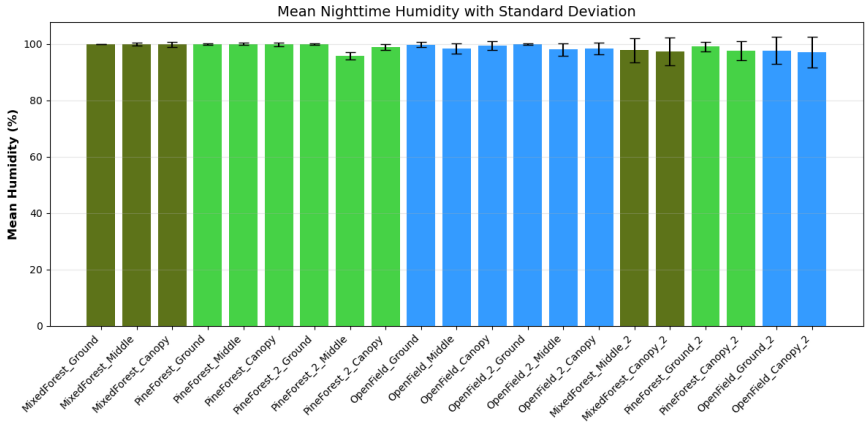

(b)

Figure 4.7.: Mean daytime (a) and nighttime (b) humidity for each sampled site, with error bars representing ±1 standard deviation. The figure illustrates humidity variability and site-to-site differences in humidity behavior at Ariel's farm.

What stands out when analysing the results from CCFC as seen in 4.8 is that cloud forests exhibit consistently higher humidity, with a mean daytime humidity of 97 percent, compared to 90 percent in pine forest and 87 percent in agricultural land. This difference can be linked to the vegetation type of cloud forest, which supports higher evaporatative capacity than either pine forest or grass land. Additionally, the dense structure of cloud forests may reduce wind penetration relative to the more open pine forests and grass lands, limiting air exchange and thereby maintaining higher humidty levels. Moreover, the figure shows smaller standard deviations in cloud forest, indicating that the fluctuations are smaller, which again, can be explained by the dense structure of the forest that creates a more stable microenvironment.

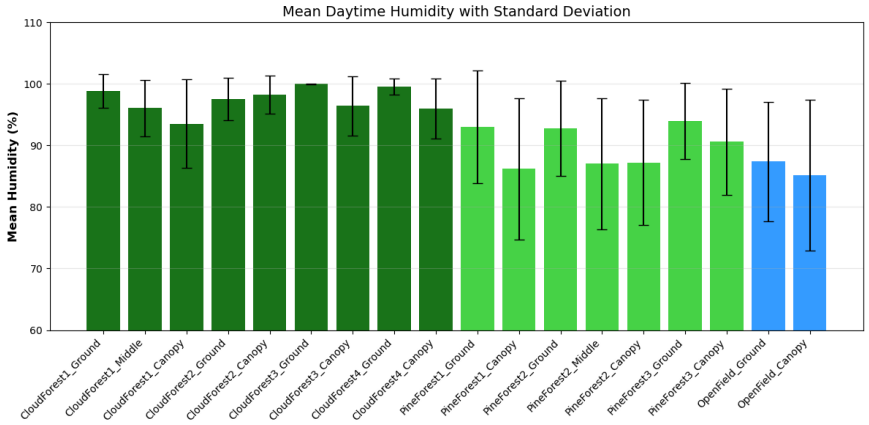

(a)

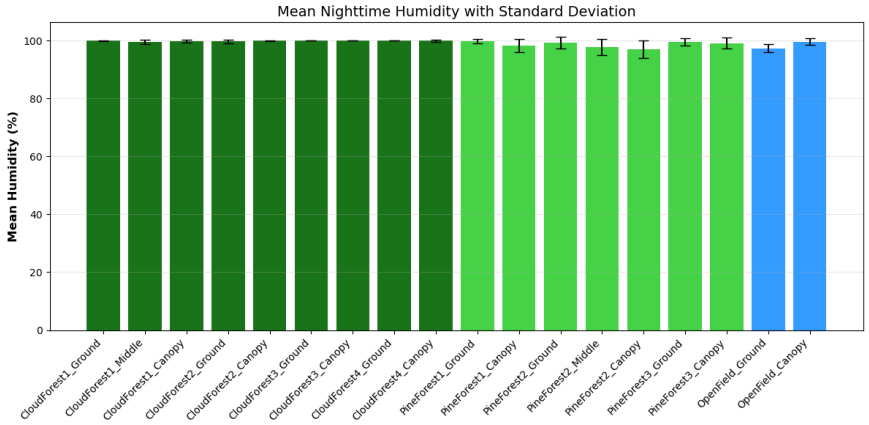

(b)

Figure 4.8.: Mean daytime (a) and nighttime (b) humidity for each sampled site, with error bars representing ±1 standard deviation. The figure illustrates humidity variability and site-to-site differences in humidity behavior at CCFC.

Figures 4.9 and 4.10 show the average daytime relative humidity levels. For Ariel's, Pine shows a higher average. This is due

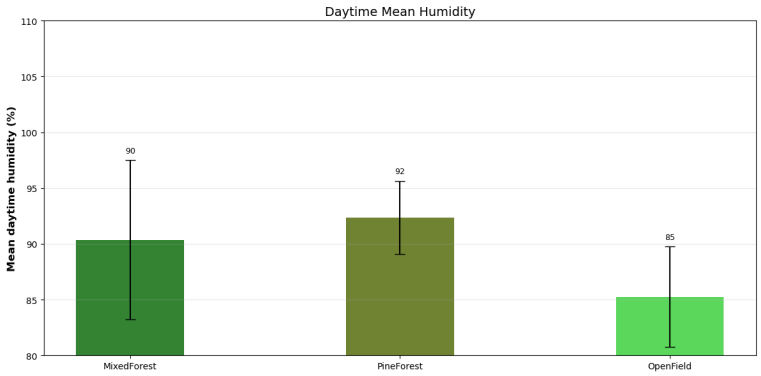

Figure 4.9.: Mean daytime humidity of land-use types at Ariel's farm.

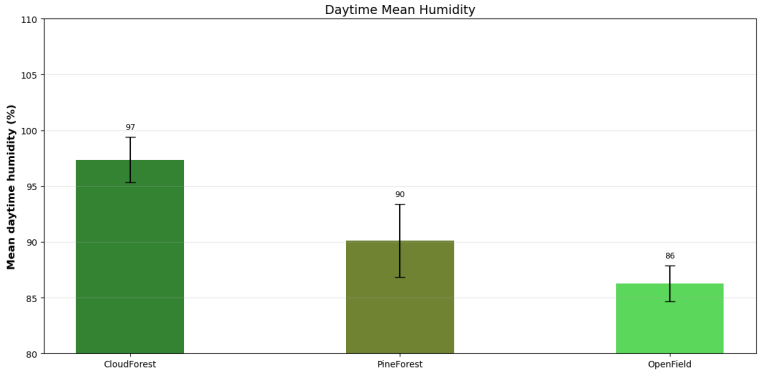

Figure 4.10.: Mean daytime humidity of land-use types at CCFC.

4.1.3. Cloud Base Height based on local Humidity and Temperature measurements

Based on temperature and humidity measurements, the LCL model provides an estimate of cloud base height, highlighting the differences between land cover types. The model used a Python script that implements a common method to determine cloud base height. It is important to note that this calculation is typically applied for open ground or grassland, largely due to relatively stable atmospheric conditions from the surface up to the top of the boundary layer. In forested areas, the microclimate can vary substantially within the canopy due to its complex structure, meaning that not all data points are suitable for accurate cloud base height calculations. Measurements taken at the top of the canopy are closest to the more stable atmosphere above the forest and are therefore used as the reference level, similar to what is done on the ground in open terrain.

Figure 4.11 shows the calculated cloud base height for Ariel's Farm and 4.12 shows the results for CCFC. As discussed earlier, the results of this calculation do not provide a precise representation of the actual cloud base height. Nevertheless, the figures demonstrate that, based on the measurements, the estimated cloud base height is generally higher in open fields and pine forests compared to mixed forests.

It should be noted that the cloud base height above the pine and mixed forest at Ariel's farm does not differ substantially. This is likely influenced by the comparatively high relative humidity of the pine forest. This contrasts with initial expectations, as the pine forest lacked undergrowth and epiphytes and would, in principle, be expected to exhibit a lower evapotranspiration capacity and evaporative flux.

The elevated humidity in the pine forest may instead be driven by topographic effects, as it is located closer to a steep valley slope, which could enhance local cloud formation through orographic lifting and forced condensation of humid air masses.

For future work, it would therefore be valuable to incorporate site-specific wind patterns (dominant wind direction and speed) and slope aspect/orientation, in order to better characterize their role in local cloud dynamics and forest microclimate regulation.

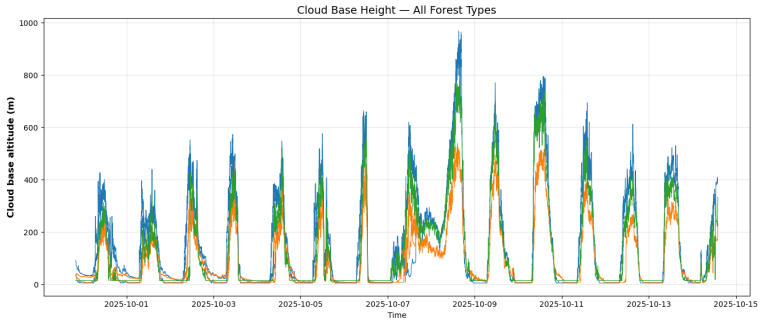

(a)

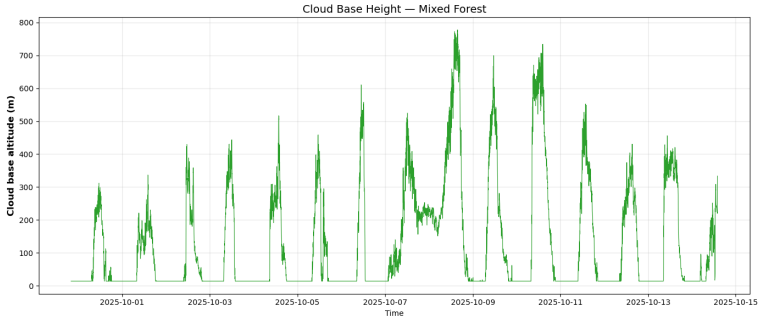

(b)

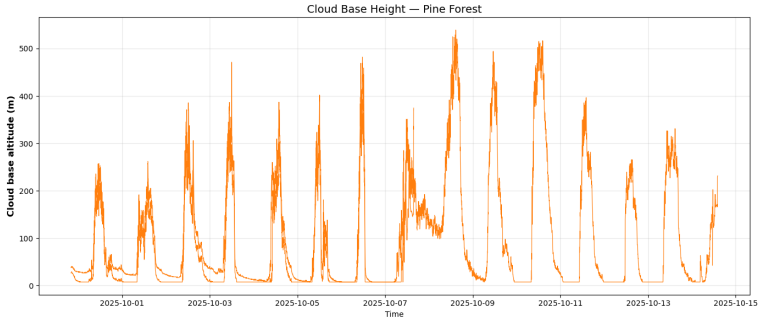

(c)

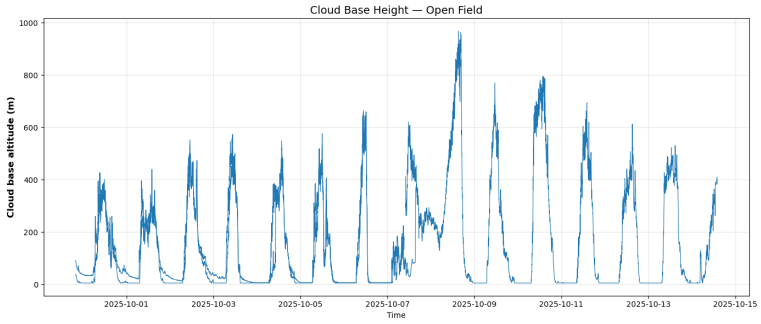

(d)

Figure 4.11.: Estimated cloud base height (CBH) derived from temperature and relative humidity measurements in different land cover types, from measurements performed at Ariel's farm. (a) shows all forest types combined, (b) mixed forest, (c) pine forest, and (d) open field. The results indicate distinct CBH patterns among land cover types, with generally lower and less variable cloud bases over cloud forests compared to pine forests and open fields.

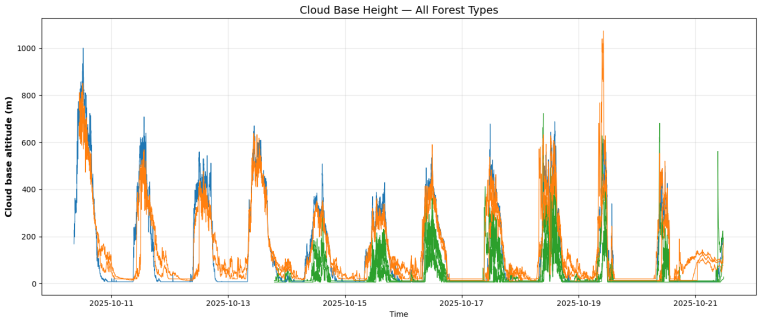

(a)

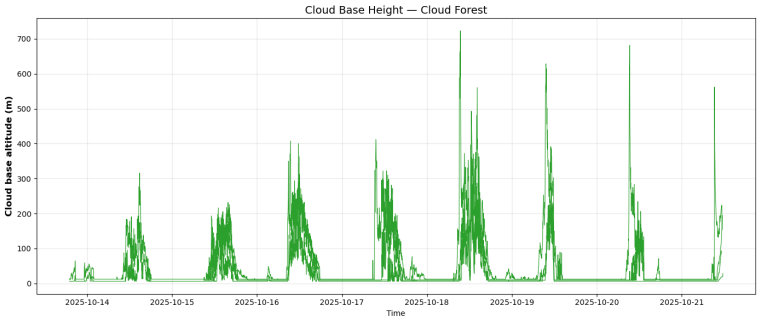

(b)

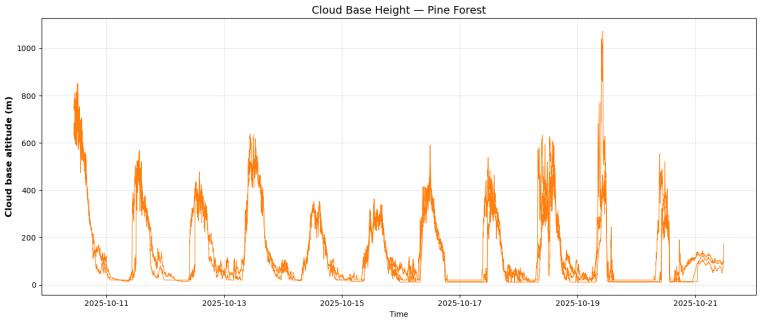

(c)

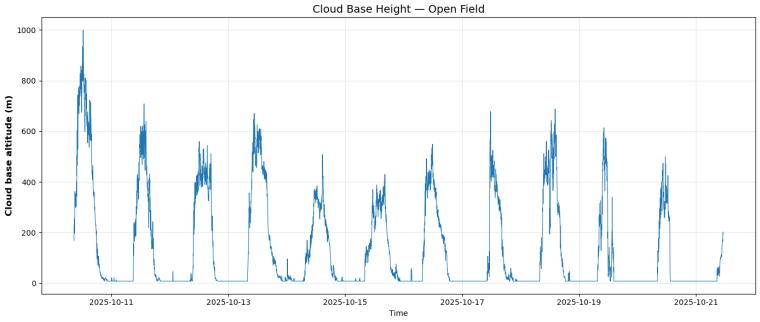

(d)

Figure 4.12.: Estimated cloud base height (CBH) derived from temperature and relative humidity measurements in different land cover types, from measurements performed at CCFC. (a) shows all forest types combined, (b) cloud forest, (c) pine forest, and (d) open field. The results indicate distinct CBH patterns among land cover types, with generally lower and less variable cloud bases over cloud forests compared to pine forests and open fields.

4.1.4. Ariel's Farm

Ariel kindly let us make use of the trees in his farm to set up our LogTags. His property was the most interesting for our analysis as there are 3 different land-use types in relative proximity to one another. We chose 2 agricultural plots of land, 2 pine, and 1 mixed. We did not choose a cloud forest plot in this case because it was not available. So instead, we chose a mixed plot which included some cloud forest trees mixed with some pine, which resembled a cloud forest but was less dense. The aim was to gather data for all three land classes and see how the same local weather phenomenon affects them.

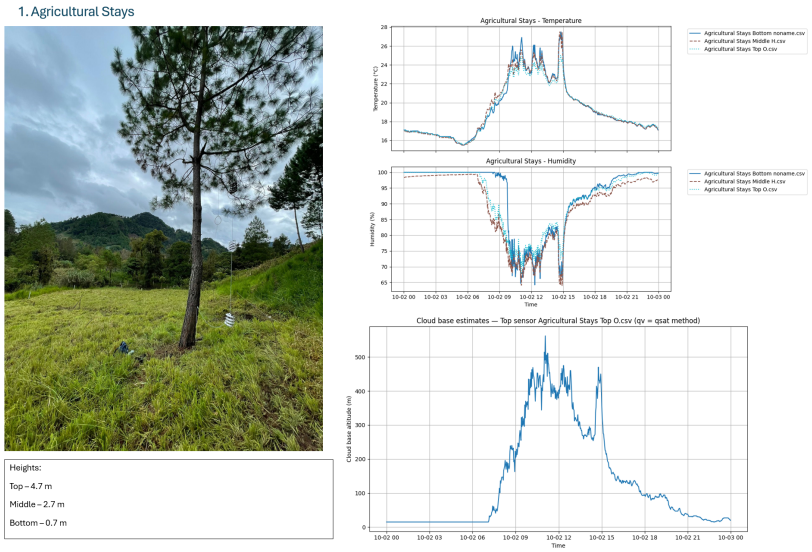

Figure 4.13.: Agricultural Stays

"Agricultural stays" is an open field on Ariel's farm with the highest sensor at 4.7 meters high. All three sensors seem to show similar temperature measurements throughout the day, with the top sensor usually being slightly colder, likely because of the canopy shading. The humidity measurements vary slightly more with height. Especially, the bottom sensor varies from 100% much later than the other two sensors. Most likely, this is due to some moisture being stuck on the sensor, which, after it evaporates, allows the sensor to measure quite similarly to the others.

The earliest time the sun affects the sensors in this case is at around 6 AM. That is when the air temperature starts to rise. It falls much more steadily, making it hard to pin point the exact time of sundown. Both temperature falls and relative humidity (RH) rise steadily after peak sun hours, until the sun rises again in the morning. There is a strong spike in temperature and dip in RH around 2:30 PM. When comparing this to the camera images taken around this time, possibly caused by a period of direct sunlight. Most of the time, this area is cloudy and thus when sunlight can shine through, it can increase air temperatures and lower RH drastically.

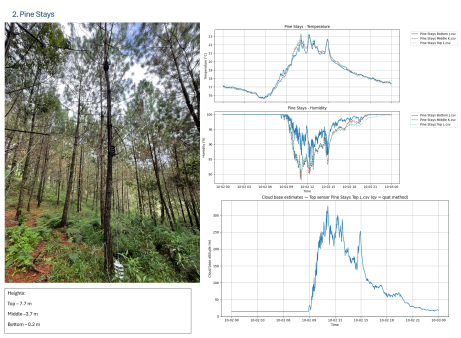

(a) Pine Stays

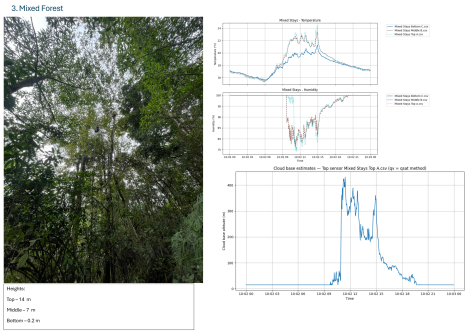

(b) Mixed Forest

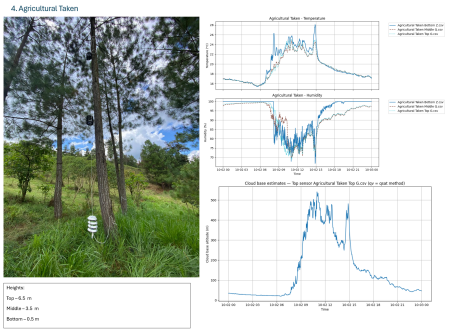

(c) Agricultural Taken

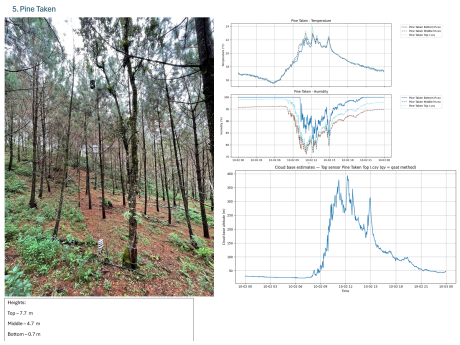

(d) Pine Taken

Figure 4.14.: Overview of all four scenes.

The cloud base height shows a similar trend to the temperature. The peak is around 500 meters at 11 PM. The other locations show a similar pattern to Agricultural Stays and are shown below. One day is used to give an intuitive overview of how one cycle would look.

This round of measurements aimed to compare 3 land use types that lie very close to each other geographically. We hypothesized that the agricultural site would have the highest temperatures, lowest humidity, and highest cloud base height. That would then be followed by the plot of pine trees and then by the mixed forest location. From the data, this is mostly correct, besides the fact that the pine tree location was much closer to the mixed forest than expected in all three categories.The following analysis will contain more plots and statistics from the entire duration of the measurement period.

The raw data looks like how we expected it to be. Temperature and humidity seem to be inversely related and show a diurnal pattern throughout the week. On the 4^{th} of October the night was much colder than usual and the humidity was therefore at 100% a bit longer.

Maximum temperatures are relatively similar for the pine and mixed forest, around 22 degrees Celsius. The maximum temperature for the agricultural area was higher, at around 26 degrees Celsius. Minimum temperatures were around 16 degrees for all plots at night. This is further evident in the mean diurnal plots for the whole week. On average, throughout the week, for all three sensors, the mixed forest has the lowest temperatures, followed closely

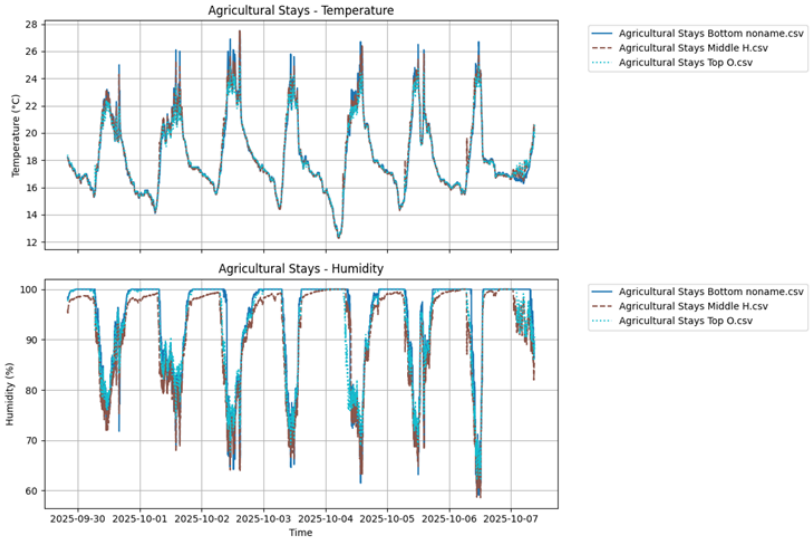

Figure 4.15.: Weekly data of the diurnal cycle of temperature and humidity at Agricultural Stays

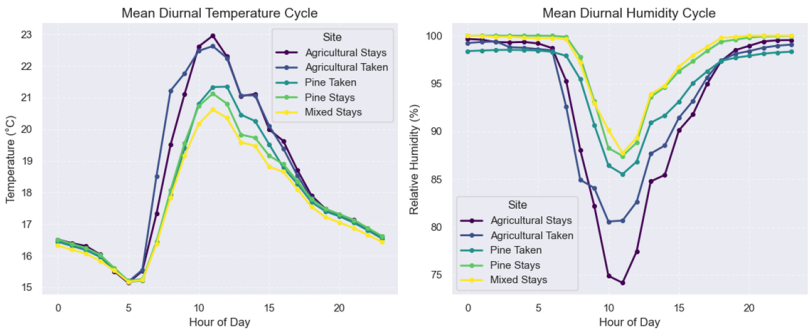

Figure 4.16.: Mean diurnal temperature and humidity at each location

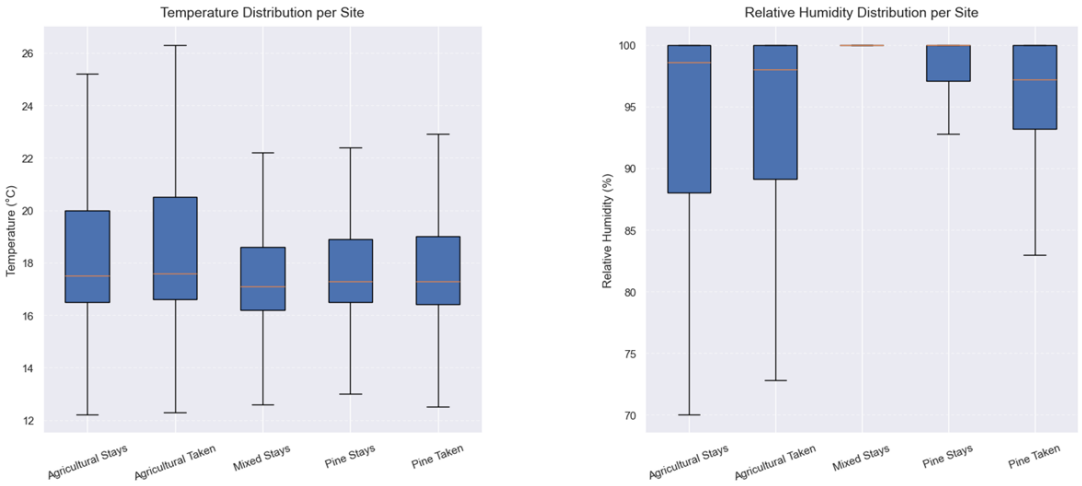

(a) Temperature ranges at each location

(b) Relative humidity at each site

Figure 4.17.: Box plots for temperature and relative humidity at all locations

by the pine forest measurements, and then by the agricultural site, showing significantly higher temperatures. The humidity shows the reverse. The agricultural site has much lower humidity, and the pine and cloud forest (or mixed) have about the same higher humidity measurements. This is shown in 4.17b plot too.

The temperature boxplots show that the minimum temperatures seem to be similar across all sites. However, what is interesting is that the top 25% of observations are much higher for the agricultural sites. This is likely because when the sun is shining on the agricultural sites, there is no shade and more mixing that causes the air below the canopies to heat up. A similar thing is shown for the humidity measurements, where the agricultural sites show the largest differences. Again, the fact that there is more mixing in these areas likely causes drops in humidity.

5. Methods: Reviewed FIESTA Model

In our research we focused on calibrating and improving the performance of the FIESTA [21] model relative to our LogTag measurements. The FIESTA model is designed to generate spatially distributed hydrological inputs, such as fog interception and Lifted Condensation Level (LCL). One of the main advantages of using a spatially distributed sensor network is that it enables verification of model predictions against real-world observations.

A key goal of our project was to compare our LogTag temperature measurements and calculated cloud base heights with those modeled by FIESTA. The acronym FIESTA stands for Fog Interception for the Enhancement of Streamflow in Tropical Areas. The model was developed by Mark Mulligan and Sophia Burke in 2005 to simulate the hydrological impacts of forest conversion in tropical montane cloud forests in Costa Rica [21]. FIESTA focuses on modeling above-ground hydrological and meteorological components for which reliable data exist, such as wind-adjusted precipitation, evaporation, fog interception, and lifted condensation level. These variables are calculated using a combination of topographic, climatic, and vegetation inputs.

Since its initial development, the Cloud Chasers I team have adapted FIESTA for the Sierra Yalijux mountain range in Guatemala, which is our own area of study. Therefore, we employ this adapted version of the model in our work.

FIESTA is particularly valuable for estimating hydrological and meteorological inputs that are difficult to measure directly, such as fog interception or spatially distributed potential evaporation. These can then be used as input to other models that for example predict streamflow, such as was demonstrated by Cloud Chasers 3, Jolijn [13].

In our research, we focus specifically on the model's output of the lifted condensation level since this was also researched using the distributed sensor network of LogTags. Additionally we make use of the modeled fog interception values to investigate temporal correlation to the canopy.

5.1. Modelling framework

Figure 5.1 shows our modeling pipeline. In this flowchart we focused on the improvement and interpretation of the FIESTA model and not on coupling its outputs to FLEXtopo.

The diagram highlights how spatial and meteorological forcing are crucial for the model outputs. It shows how our own LogTag measurements of RH and T can be used to calibrate and improve the model. Ultimately, it shows how the outputs of FIESTA can be used in a coupled model set-up together with FLEXtopo.

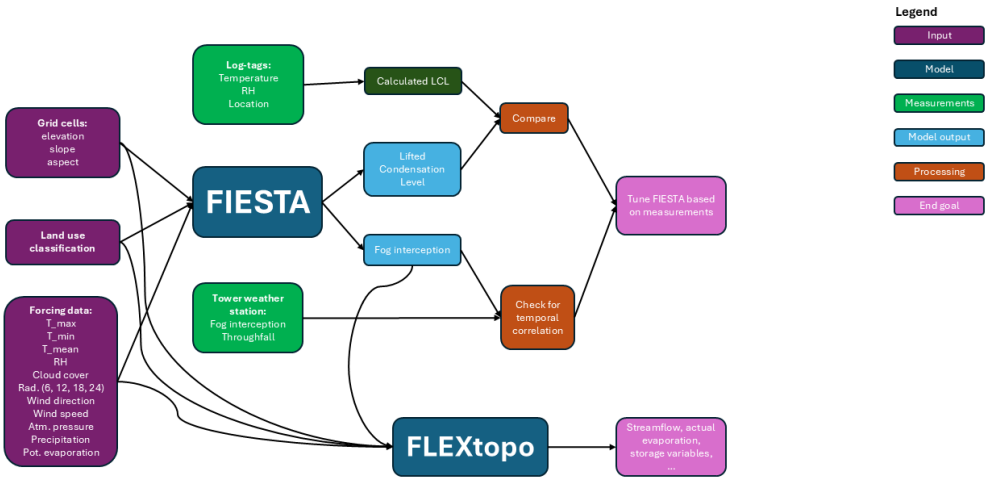

Figure 5.1.: A flow diagram showing our modelling framework.

5.2. Model set-up

The model set-up consists of four main steps. First, the spatial data are prepared using QGIS. Second, the spatial input construction for FIESTA is done. Then the meteorological forcing for FIESTA follows. Finally, the FIESTA model is adapted and spatially implemented for the CCFC catchment.

5.2.1. Spatial Data Preparation Using QGIS

The spatial foundation of the model was prepared through a structured geoprocessing workflow in QGIS, ensuring that terrain and land-cover information used in subsequent analyses was both hydrologically meaningful and internally consistent. This step is essential because the FIESTA fog-interception model is highly sensitive to topographic variability and vegetation structure, both of which must be represented with sufficient spatial detail to reflect the complexity of the CCFC catchment.

A high-resolution digital elevation model (DEM) covering the study area was first assembled and clipped to the watershed boundary. The watershed polygon was derived using HydroSHEDS drainage layers, supplemented by local flow-direction analysis to confirm the hydrological coherence of the extracted basin. To correct depressions and artifacts common in raw DEMs, the Wang–Liu sink-filling algorithm was applied, producing a hydrologically conditioned surface suitable for flow modeling.

Standard terrain derivatives such as slope, aspect, and hillshade were generated using QGIS and SAGA tools. The optimal slope algorithm values were found by comparing the different algorithms used within QGIS: GRASS, SAGA, Raster Terrain Analysis, GDAL, and the regular QGIS slope raster tool as seen in figure 5.2, from this comparison we derived that

the SAGA analysis values were most consistent and were used hereafter. We conclude this because the SAGA output follows the shape that the other options also provide with the least amount of outliers.

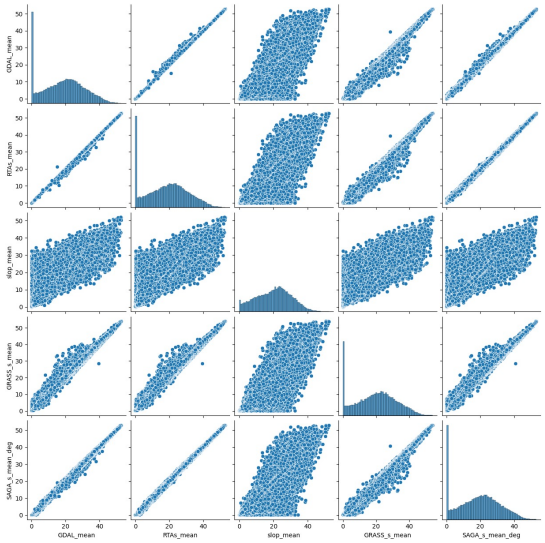

Figure 5.2.: QGIS Slope Algorithms Comparison

These variables capture the primary controls on fog exposure, wind orientation, and radiation receipt. Because fog interception is strongly modulated by slope angle and the direction toward which a surface faces, these rasters form the topographic backbone of the modeling framework. We settled on a 100 meter elevation band resolution, 45 degree aspect resolution and 5 degree slope resolution.

The continuous elevation, slope, and aspect rasters were subsequently discretized into categorical bands. This step reduces noise, facilitates aggregation, and allows terrain units to be grouped based on similar geomorphological characteristics. The discretized rasters were stacked and polygonized to generate a set of unique terrain-unit polygons, each representing a combination of altitudinal zone, slope class, and aspect sector. These polygons were assigned unique identifiers and exported for use in Python.

Land-cover characterization was performed using Sentinel-2 imagery processed with the Semi-Automatic Classification Plugin (SCP) as seen in figure 2.6. After selecting minimally cloud-contaminated scenes, the relevant spectral bands were merged into a multi-band composite. Supervised classification was carried out using manually digitized training polygons representing the three dominant land-cover classes in the area: cloud forest, pine forest, and agriculture. The resulting land-cover map was clipped to the watershed and aligned to the DEM grid. Pixel counts from each land-cover class were aggregated within terrain-unit polygons using QGIS's Zonal Histogram function, and the resulting tables were exported for integration into the spatial input generation notebook.

The spatial datasets used as inputs to the Python processing pipeline were derived from two primary sources: a 30-m resolution DEM and a 10-m resolution Sentinel-2 land-cover classification. Terrain attributes (elevation, slope, aspect) therefore reflect the coarser 30-m topographic grid, while vegetation fractions were computed from the finer 10-m classified

imagery. These raster inputs were subsequently aggregated into terrain classes, forming the spatial units through which the adapted FIESTA model represents fog interception and surface–atmosphere interactions.

The combined QGIS workflow thus produced: (i) hydrologically corrected terrain derivatives, (ii) discretized terrain-unit polygons, and (iii) terrain-unit-specific vegetation fractions. These datasets serve as the essential spatial inputs for the subsequent model processing.

5.2.2. Spatial Input Construction for FIESTA

After preparing the spatial foundation in QGIS, the next step is to convert these terrain units into the parameter tables needed by FIESTA. The notebook *creatingspatialinputfile.ipynb* translates the QGIS-generated terrain and land-cover datasets into the spatial parameter tables required by the FIESTA fog-interception model. FIESTA operates most effectively when the landscape is represented not as individual pixels but as aggregated terrain units defined by consistent geomorphological and vegetation characteristics.

The workflow begins by importing the discretized elevation, slope, and aspect classes for each raster cell, along with planimetric area and preliminary land-cover assignments. Because fog deposition depends on the true exposed surface area rather than horizontal projection, the notebook computes the three-dimensional surface area for each pixel by correcting for slope. This adjustment appropriately increases the effective surface area in steep terrain and is essential for realistic fog interception and radiation calculations.

Next, pixels are grouped into unique combinations of elevation class, slope class, and aspect class. For each terrain unit, the notebook calculates: the number of contributing pixels, representative geometric properties, total 3D surface area, relative area weight (cell-size factor). This aggregation condenses the landscape into a manageable set of terrain units while maintaining the spatial diversity characteristic of CCFC's mountainous environment.

Land-use fractions are then assigned to each terrain unit using one of two approaches. A preliminary method infers vegetation composition from elevation alone; this was the approach taken in Jolijn Hiemstra's Masters Thesis work, but the preferred approach for our study integrates the SCP-derived land-cover map. For each terrain unit, pixel counts of cloud forest, pine forest, and agriculture are converted into fractional coverage. These fractions determine the structural characteristics of vegetation leaf area, canopy roughness, and forest edge length that directly influence fog interception efficiency.

The final output is a spatial input table listing terrain-unit properties (elevation-band, slope class, aspect class, planimetric area, 3D area) along with fractional vegetation cover. This table is formatted to interface with the FIESTA model and serves as the spatial backbone for simulating fog deposition patterns across the catchment.

5.2.3. Meteorological Forcing Preparation for FIESTA

Once the spatial forcing files are in order, we have to create the necessary meteorological input files for the model.

The notebook *inputfiles.ipynb* produces the meteorological forcing data necessary for driving FIESTA. Since fog interception is closely linked to temperature, humidity, wind, surface

pressure, and radiation, preprocessing of meteorological observations must be rigorous and hydrologically appropriate.

Raw measurements from the INSIVUMEH Coban weather station including temperature, relative humidity, wind speed and direction, cloud coverage and rainfall were imported. Since the meteorological parameters that INSIVUMEH shares change over time we were not able to acquire a complete meteorological forcing dataset from INSIVUMEH alone. Two other necessary inputs, incoming radiation and atmospheric pressure, thus had to be imported from a weather station based on CCFC campus. In order to minimize unwanted mixing of weather station data we chose to use data from a Tempest weather station located at CCFC campus near a living cabin. We needed to supplement this data with cloud cover from the INSIVUMEH weather station, as this variable was not registered. Secondly, we replaced the daily precipitation variable with the one caught by the tower weather station as the Tempest weather station has proven to not reliably catch this parameter.

After merging the data was subjected to temporal cleaning and quality control. Timestamps are harmonized, missing values are identified, and spurious readings are removed. The cleaned dataset is resampled to a daily timestep using hydrologically relevant aggregation rules: daily minimum, mean, and maximum temperature; mean humidity and pressure; total rainfall; and dominant wind direction and magnitude.

Radiation is processed in a manner consistent with the requirements of the original FIESTA framework. Instead of a single daily value, the notebook extracts short-window averages centered around four characteristic times (approximately 00:00, 06:00, 12:00, and 18:00). These temporal slices preserve the essential shape of the daily radiation curve and allow the model to respond to mid-day clearing and afternoon cloud formation distinctive features of cloud-forest microclimates.

All processed variables are compiled into a standardized daily forcing file containing: Year, Month, Day, Tmin, Tmax, Tavg, RH, Rad24, Rad6, Rad12, Rad18, Wndd, Wndspd, Presh, Prcp.

This file directly drives the fog-interception and energy-balance calculations in FIESTA.

To support sensitivity experiments, the notebook also generates a monthly climatology derived from long-term INSIVUMEH records. These climatological means provide a smoothed representation of typical atmospheric conditions and can be used to test the model under synthetic climate scenarios.

5.2.4. Adaptation and Spatial Implementation of the FIESTA Model in the CCFC Catchment

With the different inputs arranged, it is time to look at the model itself. In this project, the FIESTA model is reconfigured to operate as a fully spatial, terrain-class based hydrological model, capable of resolving daily fog deposition and evaporation across the complex topography of the CCFC watershed. The notebook *FIESTA3landclasses.ipynb* introduces several advancements that expand spatial granularity of the original framework. The elevation, slope, and aspect of each terrain unit are derived from a high-resolution DEM that is clipped to the local watershed boundary. These topographic attributes govern air uplift, wind exposure, and solar energy receipt, all of which directly influence fog formation and moisture exchange. In the mountainous environment surrounding CCFC, small differences in slope

orientation can produce large differences in fog interception potential, making spatial representation essential for accurate hydrological modelling.

Meteorological inputs were also refined beyond the original implementation. While earlier applications relied primarily on consistent but spatially coarse weather-station records, the present version incorporates multiple atmospheric measurements, including station temperature and humidity, corrected precipitation, wind speed, and direction. Missing values were reconstructed by temporal interpolation to ensure continuity. Using these variables, the model computes the lifting condensation level (LCL) for each day, allowing cloud base height to rise and fall dynamically. When terrain lies at or above the LCL, the model interprets it as being immersed in cloud, creating the physical conditions necessary for fog deposition. The absolute humidity and liquid water content of the fog layer are calculated from temperature and vapour pressure, enabling the model to represent how atmospheric moisture availability changes with synoptic conditions.

Earlier versions of FIESTA use distinguish only between broad forest and non-forest categories. In contrast, this project uses land-cover fractions derived from Sentinel-2 supervised classification to assign each terrain class a unique mixture of cloud forest, pine forest, and agriculture. These fractions directly determine leaf-surface area, canopy roughness, and forest edge length, all of which control the pathways of the model through which fog water is captured. Cloud forests, with dense, rough canopies and high leaf area, are represented as highly efficient fog collectors, while pine stands have a different aerodynamic structure, and cleared land contributes little to interception. The model calculates both vertical droplet settling and horizontal wind-driven impaction on vegetative surfaces, incorporating how slope orientation modulates wind exposure. In this sense, vegetation forms an active hydrological agent rather than a static land-cover label.

Radiative and energy processes are similarly integrated. The model divides the day into four time periods corresponding to the available radiation measurements and modifies each by slope, aspect, fog immersion, and cloud cover to compute net radiation. This governs the atmospheric demand for evaporation. Fog immersion both reduces solar energy and increases moisture availability, meaning that foggy days typically depress evaporation while simultaneously increasing water inputs through deposition. The model's coupling of radiation and canopy water exchange allows these compensating effects to be simulated.

For each day, fog deposition, precipitation, and actual evaporation are combined into a daily water budget for every terrain class. Positive values reflect moisture surplus, while negative values indicate atmospheric demand exceeding inputs. Through this mechanism, the model resolves how water availability shifts across the catchment under different climatic and land-cover conditions.

Ultimately, this adaptation preserves the physical foundations and empirical strengths of the original FIESTA model while extending its applicability to catchment-scale, spatially resolved assessments. It produces a set of daily outputs fog deposition, evaporation, energy balance, and net moisture inputs that reflect both the microclimatic variability of the region and the dynamic ecological configuration of the landscape. These capabilities are essential for understanding the sensitivity of fog-dependent hydrological systems to climate variability and land-use change.

5.3. Calibration and results

Using the data from the distributed sensor network, several adjustments were made to calibrate the FIESTA model and improve its ability to show the lifted condensation level.

- Improve the land-use based temperature and RH shift-parameters.
- Change the function used to calculate LCL.
- Add a diurnal pattern for relative humidity based on daily data.

These are the initial data for measured (blue) and modeled (yellow) temperature and humidity. This will then be a reference for the upcoming calibrations. The scatter plots in figure

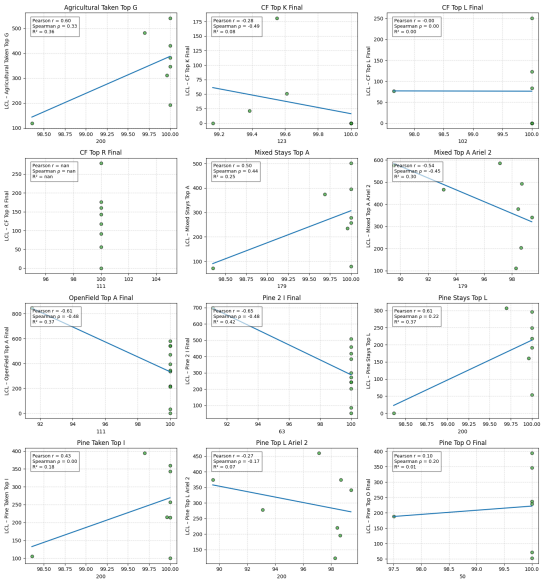

Figure 5.3.: Scatter plots of modeled vs measured cloud base height

5.3 show the relationships between the modeled and measured data for each location. The initial correlation is not showing a strong relationship. Average pearson correlation equals -0.01, spearman correlation averages at -0.08 and R2 is 0.22.

Graphs 5.4 and 5.5 show that the modeled temperature seems to be overlapping quite well with the measured data and that the relative humidity is still quite far off compared to the measured RH. The modeled humidity is much lower and is not able to capture the diurnal variation.

5.3.1. Improved land-use based temperature and RH shift-parameters.

The first adjustment made to the FIESTA model consisted of using our measured relative humidity values inside the model. We updated the python function `T_lucc_shift` that shifts the temperature per grid cell based on the fraction of cloud forest present. The new parameter value of -1.5 degrees Celsius is justified based on the average temperature differences

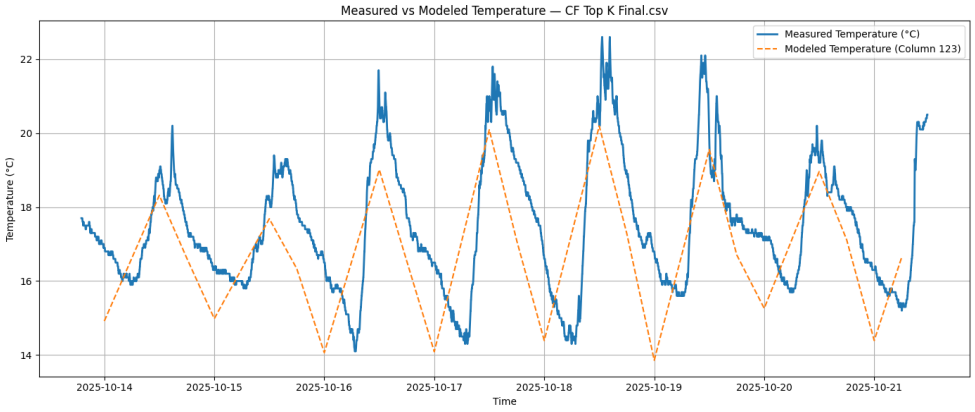

Figure 5.4.: Modeled vs measured temperature for cloud forest measurements

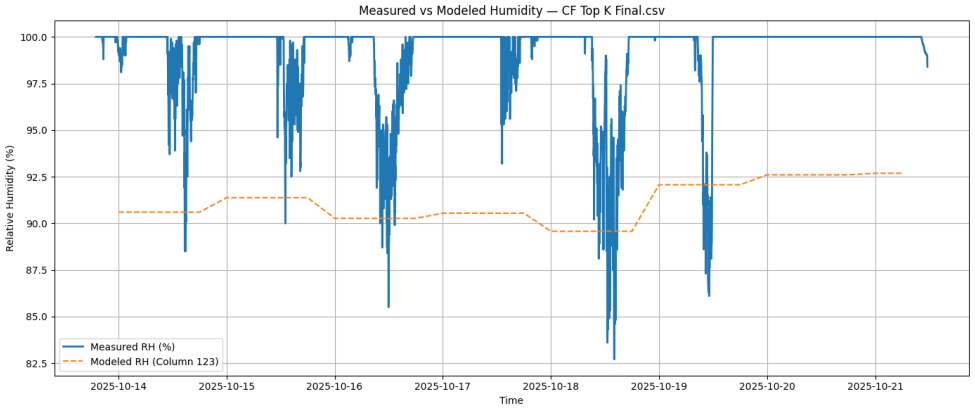

Figure 5.5.: Modeled vs measured humidity for cloud forest measurements

between land use classes, as described in section 4.1.1, and the location where our main data source of forcing data can be found. The main source for our forcing data is the weather station at the CCFC cabin, this is located in an area of the CCFC campus that is mostly an open field with some loose trees. Secondly, we observed that the standard deviations for the average daytime mean temperatures for cloud forest and open field had values of respectively. These variances are not extremely large.

Therefore, we decided to set the average temperature shift slightly lower than the average difference of -1.8 degrees between cloud forest and open field. Next to this we added a function `RH_lucc_shift` which shift the relative humidity for a given grid cell based on the land use type. Here we use section 4.1.2 to set up an average shift of 7% for a grid cell consisting fully of cloud forest.

Figure 5.6 shows a moderate correlation between the measured and modeled variables. With some exceptions include the final cloud forest measurement with LogTag K, because most of the RH measurements were 100 percent even during the day.

Graphs 5.7 and 5.8 show the measured vs modeled temperature and humidity after the shift. The humidity here is already much better, with it being at 100 percent most of the

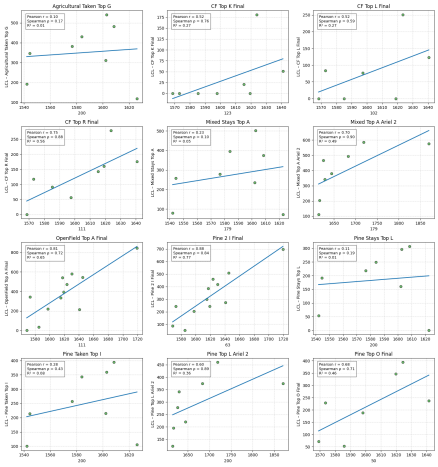

Figure 5.6.: Scatter plots of the T and RH shift

time. There is, however, still no diurnal variation, which would be important to discuss the cloud base height during the daytime.

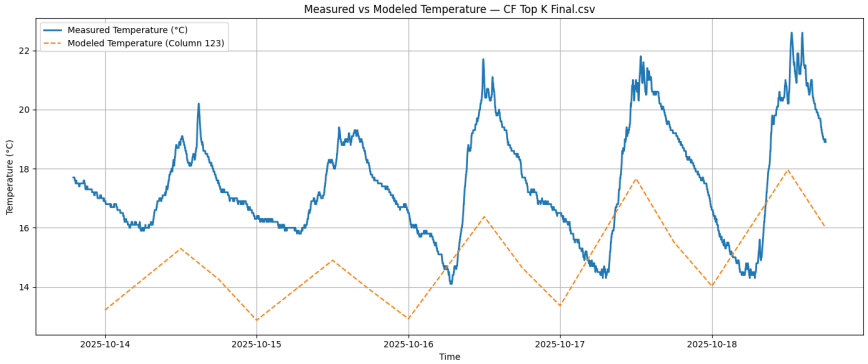

Figure 5.7.: Measured vs modeled temperature after shift

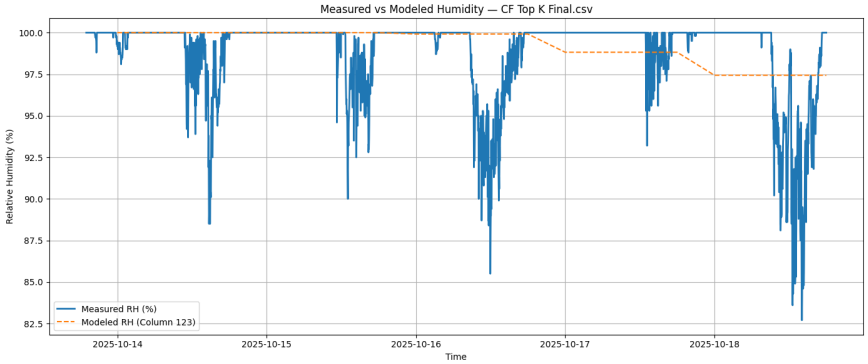

Figure 5.8.: Measured vs modeled humidity after shift

Overall we see an average pearson correlation of 0.49 between the modeled and measured LCL values. The spearman correlation equals 0.44 and we have an R2-value of 0.32 on average. These pearson and spearman correlation values indicate that even though FIESTA is able to capture the general direction and trend of changes, we are not yet able to capture the magnitude of change. The R2-value of 0.32 supports the conclusion that we are not yet able to capture much of the variance.

5.3.2. Changing the function that is used to calculate LCL

The second adjustment made involved changing the way that the Lifted Condensation Level was calculated in the python function `LiftingCondensationLevel`. In the initial version we used the version that was employed in FIESTA by the first Cloud Chasers group. This method consists of calculating the dew point temperature based on the saturated vapor pressure, and after this multiplying the difference between the measured ground temperature and the dew point temperature with an empirical factor which was set at 125. In the updated version, we implement the method described in section 2.5 to determine the Lifting Condensation Level (LCL). This method calculates the height at which an air parcel becomes saturated by first iteratively lifting the air parcel through different atmospheric levels and computing the saturated vapor pressure at each height using the Clausius-Clapeyron equation. We then compare the actual vapor pressure (which remains constant during dry adiabatic ascent) with the saturated vapor pressure at each level. Lastly, we identify the condensation point where the actual vapor pressure equals or exceeds the saturated vapor pressure. The method steps through height increments, applying adiabatic cooling to calculate temperature changes with altitude, until we find the level of saturation. This iterative approach provides a more accurate determination of the lifted condensation level than our previous simplified analytical approximations.

The scatter plots in figure 5.9 show the relationships between the modeled and measured data for each location. The correlation is still not showing a very strong relationship. Average pearson correlation equals 0.48, spearman correlation averages at 0.46 and R2 is still 0.33.

5.3.3. Adding a diurnal pattern for relative humidity based on daily data

Our third adjustment consists of adding a diurnal pattern to the relative humidity parameter. When observing the lifted condensation level, but also temperature and relative humidity values that were observed and calculated using the logtags, there is a clear diurnal pattern visible. The FIESTA model is able to emulate this into its temperature observations inside the python function `Temps`. Inside `Temps` the daily minimum and maximum temperature from the meteorological forcing data are used to create a diurnal temperature range. This range is then used to synthetically recreate the diurnal pattern.

06:00: $T = \bar{T} - 0.25\,\Delta T_{\text{diurnal}}$
12:00: $T = \bar{T}$
18:00: $T = \bar{T} + 0.25\,\Delta T_{\text{diurnal}}$
24:00: $T = \bar{T}$

FIESTA does not capture the diurnal pattern in LCL if this is only present inside its temperature values. To allow FIESTA to capture the diurnal pattern for both the RH and LCL we have implemented a similar function called `RHDiurn` for the relative humidity. First, the

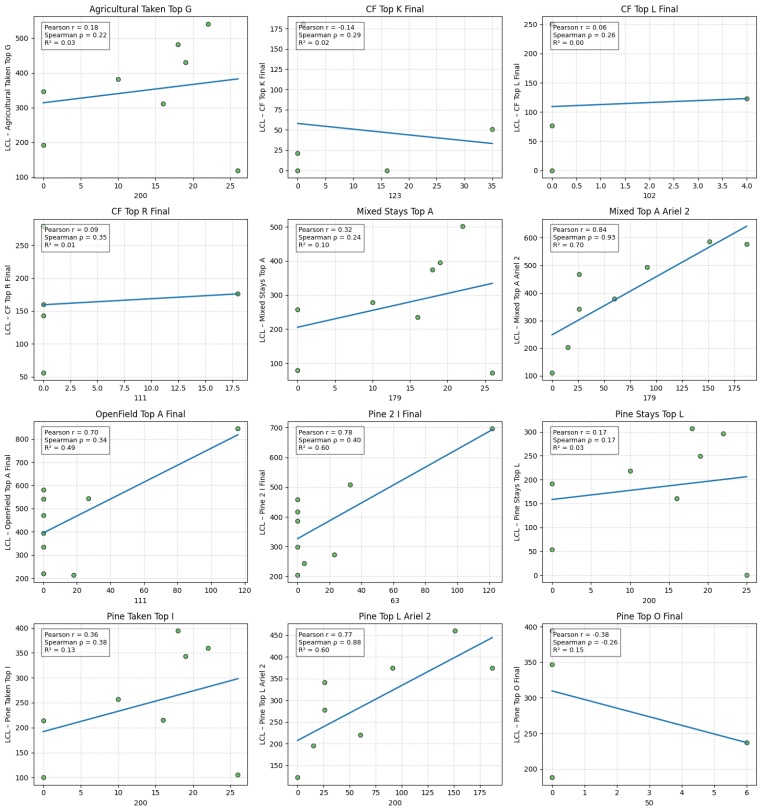

Figure 5.9.: Scatter plot of modeled vs measured values using the new LCL calculation

meteorological forcing needed to be expanded by adding a daily minimum and maximum of the RH. This means that this function cannot be created using the INSIVUMEH data as a base, since they only provide daily mean RH measurements.

Next, using this minimum and maximum daily relative humidity we create a daily diurnal range and assign RH values to the four daily timestamps.

06:00: $RH = \bar{RH} - 30\,\Delta RH_{\text{diurnal}}$
12:00: $RH = \bar{RH}$
18:00: $RH = \bar{RH} + 0.30\,\Delta RH_{\text{diurnal}}$
24:00: $RH = \bar{RH}$

The scatters plots in figure 5.10 show a much better linear relationship. This indicates that the adjustments allow FIESTA to model the cloud base height at our locations much more accurately. This is mostly because it increases the quality of our forcing data, which is shown below. In terms of outcomes we observe that after implementing a diurnal RH pattern we have an average pearson correlation of 0.67, an average spearman correlation of 0.62 and an R2-value of 0.47. These improved correlation values mean that with a diurnal RH-pattern FIESTA is able to capture the size of the LCL a lot better. Additionally the new R2-value of 0.47 indicates that around half of the variance in our measurements can be explained by FIESTA.

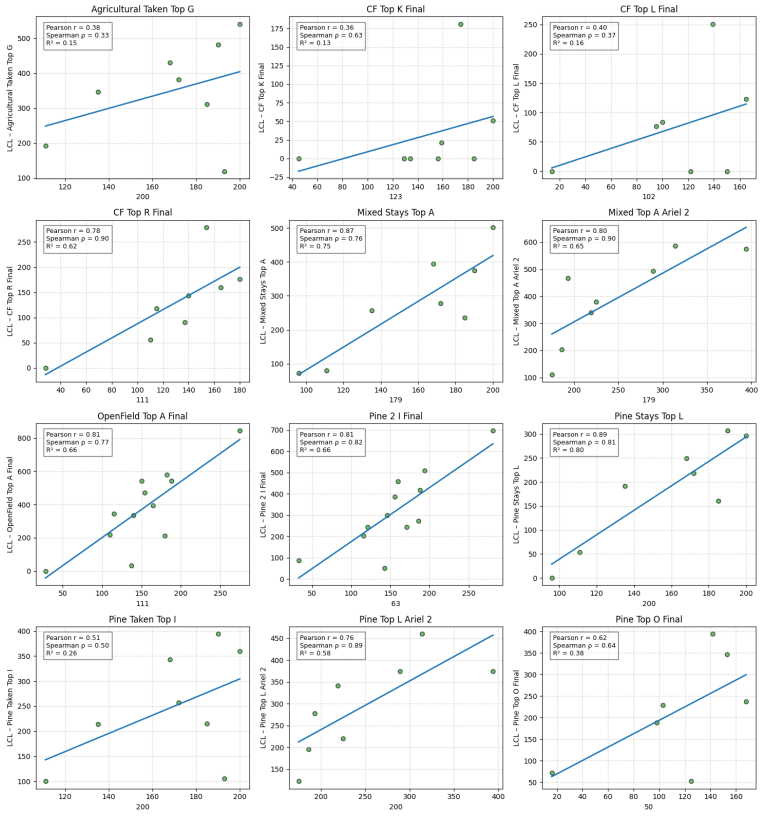

Figure 5.10.: Scatter plots of modeled vs measured values after all adjustments

The raw data in figures 5.11 and figures 5.12 show a much better situation than before the adjustments. Now the magnitudes of the values overlap much more nicely. These adjustments are essential to allow FIESTA to model accurate cloud base height for Rubel Chaim and our other locations.

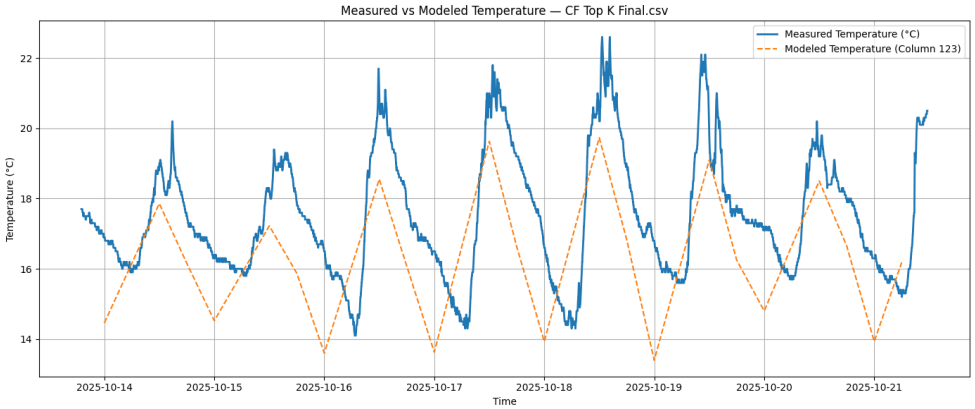

Figure 5.11.: Modeled vs measured temperature after diurnal cycle adjustment

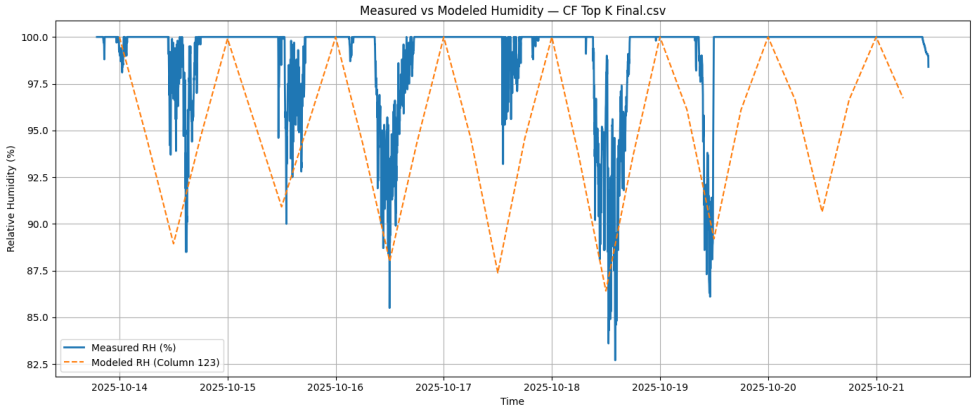

Figure 5.12.: Modeled vs measured humidity after diurnal cycle adjustment

5.3.4. Fog trap correlation

When correlating the results of our FIESTA modeling to the results of the fog trap at the tower there is no apparent correlation at 0.03. This is visible in figure 5.13.

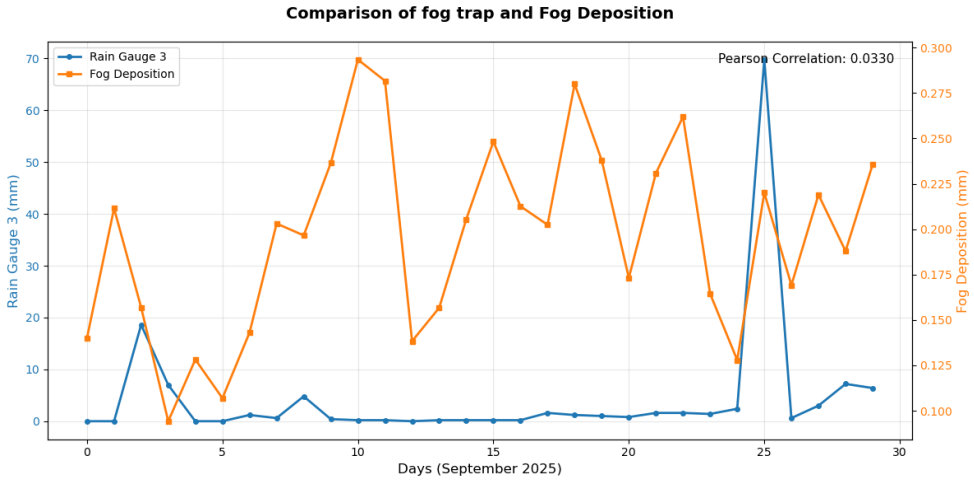

Figure 5.13.: A plot showing our modeled fog interception against values measured at the meteorological tower.

One source of this error might lie in the fact that the fog trap located at the tower appears not to be functioning well. It has been reporting peaks of well over 10 mm of fog per day at its peak which is way outside of the realistic range. This is likely due to precipitation that is raining into the fog trap.

Additionally, after filtering the peaks out there is also still a very low correlation at 0.10.

5.4. FIESTA conclusion

This study evaluated and adapted the FIESTA model for application in the CCFC catchment by calibrating its temperature, humidity, and cloud-base height formulations using observations from our distributed sensor network. The primary goal was to improve the model's ability to reproduce the lifted condensation level (LCL), a key driver of fog immersion and fog interception processes in cloud-forest environments.

The initial comparison between modeled and measured temperature and relative humidity showed that FIESTA already reproduced temperature patterns across land-use types with reasonable accuracy, while modeled humidity lacked both magnitude and diurnal variability. We set out to correct these weak spots inside the model.

The first improvement involved implementing land-use-dependent temperature and humidity shift parameters. Updating the function `T_lucc_shift` with a revised shift of -1.5°C and introducing a new `RH_lucc_shift` function enhanced how FIESTA captures meteorological conditions across vegetation types. These modifications produced moderate correlations between modeled and measured values and reduced systematic biases, particularly in the cloud forest where humidity tends to be persistently high.

The second adjustment replaced the simplified analytical LCL formulation previously used in FIESTA with an iterative saturation-based method. By lifting an air parcel through the atmospheric column and computing saturation conditions using the Clausius–Clapeyron relation, this updated implementation provided a more physically consistent estimate of LCL. Although this refinement yielded only modest improvements in correlation (average Pearson ≈ 0.48, Spearman ≈ 0.46, $R^2 \approx 0.33$), it established a more robust physical foundation for subsequent enhancements.

The most substantial improvement resulted from adding a diurnal cycle to the relative humidity forcing. By extending the meteorological input data to include daily minimum and maximum RH values, and implementing the `RHDiurn` function to generate a synthetic daily cycle, FIESTA became sensitive to the daytime rise and nighttime collapse of the LCL. This adjustment addressed a key limitation of the previous model version, which could not capture any temporal structure in humidity beyond a daily mean.

After incorporating the diurnal RH pattern, the agreement between modeled and measured LCL improved markedly. The average Pearson correlation increased to 0.67, the Spearman correlation to 0.62, and the coefficient of determination to $R^2 = 0.47$. These results indicate that FIESTA is now able to capture not only the general direction of LCL variability but also a substantial portion of its magnitude and temporal dynamics. Approximately half of the observed variance in LCL can now be explained by the model, this is an important improvement given the complexity and heterogeneity of cloud-forest microclimates.

Together, these adjustments demonstrate that FIESTA's atmospheric components can be meaningfully refined when supported by spatially distributed field measurements. Although FIESTA remains fundamentally a hydrological model, its ability to estimate fog-relevant atmospheric drivers, particularly LCL, directly influences the accuracy of fog interception and, ultimately, catchment-scale hydrology. By improving the representation of temperature, humidity, and cloud-formation processes, this study strengthens FIESTA's suitability for application in fog-dependent tropical montane ecosystems.

Overall, this work extends the usability of FIESTA by enhancing its representation of cloud-terrain interactions and microclimatic controls on fog formation. The improved forcing data

and atmospheric formulations create a more reliable and accurate basis for future hydrological modelling, including fog interception estimates, flow simulations, and scenario analyses exploring land-use change and climate sensitivity at the CCFC and similar cloud-forest catchments.

Next steps should include looking into how to improve the quantification of fog interception. Additionally, in the current set-up of the model we make use of four timesteps that are evenly spaced starting at 0:00 with 6 hours in between. Future should look into how these timing steps and starting points can be optimized to represent the actual diurnal pattern, smaller discretizations could be used as well as a different timing for peak temperature and RH. We observe that RH dynamics are insufficiently caught by the current model as they show large time periods of being at maximal value.

6. Canopy water balance and microclimate

The first part of this report was dedicated to gaining a better understanding of how the lifted condensation level can be determined. As earlier explained, an elevated LCL lowers the fog interception ability of a cloud forest. To link the lifted condensation level to hydrological cycle we will introduce a canopy water balance model in this chapter.

This analysis is structured by first using the canopy balance model to assess data reliability (e.g. whether the canopy water balance monitoring tower can help in understanding fog events). Second, it evaluates whether the instruments installed in the tower function consistently through implementing the canopy water balance model. After that, microclimate variation across the CCFC campus were briefly explored and compared to how these relate to our LogTag measurements.

6.1. Fog events

6.1.1. Tower measurements

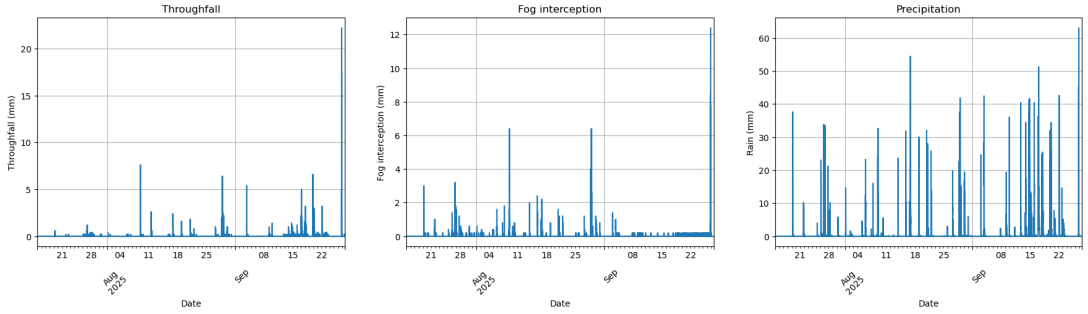

(a) Throughfall (b) Fog interception (c) Precipitation

Figure 6.1.: Data measured by the in-canopy weather station on top of the tower.

Figure 6.1 shows throughfall, fog interception and precipitation as measured by the weather station. The precipitation and fog measurements were made on top of the tower at a height of 13,5 meters and the throughfall set-up is located at ground level. A diagram of the tower set-up is visible in figure 6.4a.

The start of the project was in sync with the start of the rainy season. Both the intensity and frequency of precipitation events increased during this period. Throughfall rises accordingly while the magnitude of fog interception seems to decrease over time. Several fog interception

peaks are unrealistically large which is most likely caused by rainfall entering the fog trap. Despite the decrease in intensity, the frequency of fog events appears to increase.

To further inspect the behavior of the system, we highlight two specific cases shown in the figures below.

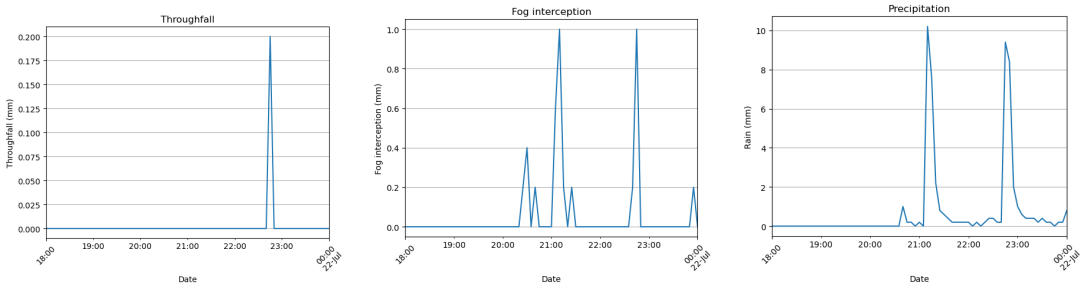

(a) Throughfall (b) Fog interception (c) Precipitation

Figure 6.2.: Data from 21 July, 18:00–24:00.

Figure 6.2 highlights a case where the fog trap begins recording roughly half an hour before the rain gauge detects precipitation. This indicates that the canopy was already immersed in a saturated air mass, allowing horizontal precipitation to occur before the start of vertical rainfall. Such timing differences are typical in cloud forests, where cloud immersion and rainfall do not necessarily coincide. This reinforces the idea that fog deposition represents an independent hydrological input that would remain invisible without dedicated in-canopy instrumentation.

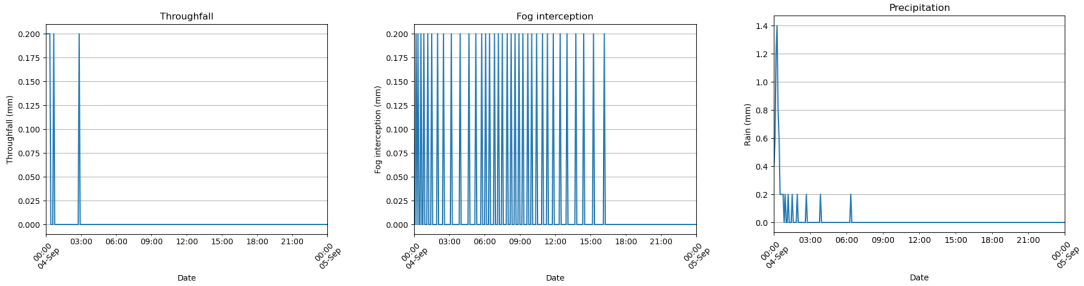

(a) Throughfall (b) Fog interception (c) Precipitation

Figure 6.3.: Data from 4 September.

Figure 6.3 shows the opposite situation: fog interception continues for nearly ten hours after a brief rain event that produced only short-lived throughfall. This indicates that the canopy remains coupled to a supersaturated layer despite the rainfall. The examples of the two sensors provide evidence that the processes governing rainfall and fog deposition operate at least partly independently.

Both Figure 6.2 and Figure 6.3 highlight the importance of understanding fog interception as a hydrological input separate from rainfall.

6.2. Canopy water balance model

This section discusses the canopy water balance model that we set-up based on the structure that CCIV created.

6.2.1. Forcing and model description

The forcing data for the canopy balance model consist of daily time series of precipitation, throughfall, temperature, relative humidity, solar radiation and wind speed. Precipitation includes both vertical and horizontal components, and daily evaporation is calculated using the Penman–Monteith equation.

The model is a bucket-type water balance model consisting of five storage components:

- Dynamic interception (limited by dynamic canopy capacity)
- Static interception (limited by static canopy capacity)
- Forest floor storage, receiving throughfall and stemflow
- Unsaturated soil, where evapotranspiration occurs
- Saturated soil, receiving deep drainage

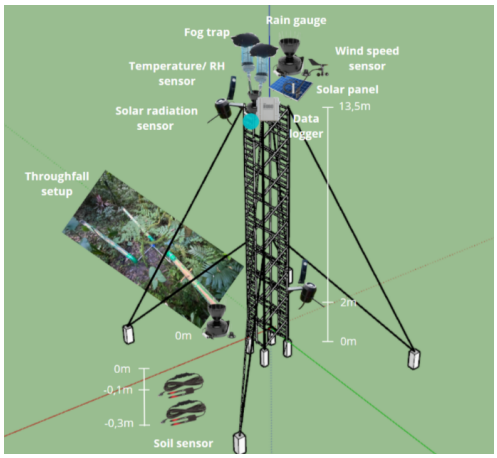

(a) Diagram of the tower with sensor locations [42]

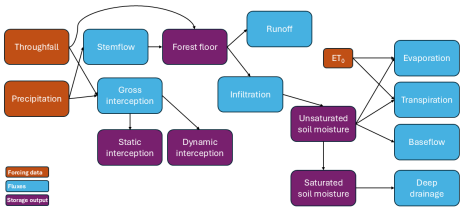

(b) Flowchart of the canopy balance model.

Figure 6.4b summarizes the model workflow and shows a diagram of the in canopy tower set-up with the locations of all the sensors. The resulting model output can be found in Figure 6.6.

The saturated soil moisture content increases steadily during the study period, while the unsaturated layer oscillates within a stable range. Correlations between model storage components and precipitation remain low (around 0.15), as shown in Figure 6.8, indicating that interception and soil thresholds buffer the daily soil response.

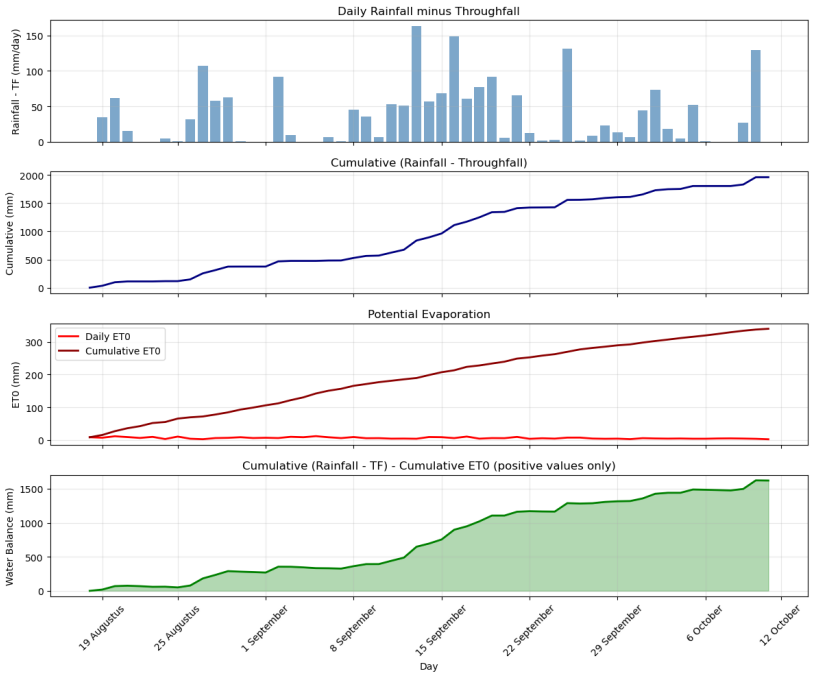

Figure 6.5.: Daily gross interception and evaporation, combined with cumulative sums and the increase in the water balance.

Figure 6.5 illustrates the basic partitioning between rainfall, throughfall and potential evaporation. It indicates a massively large and unrealistic accumulation in the water balance, of around 1500 mm over a period of around eigH weeks. We suspect that the issue lies in an underestimation of the throughfall. This underestimation leads to a non reasonable value for the gross interception. We can link the malfunctioning of the throughfall measurements to our own observations in Guatemala where we noticed that maintenance was not carried out regularly which allowed for cluttering by leafs and other rubble.

Gross interception is computed as precipitation minus throughfall and then partitioned into static and dynamic interception with capacities of 1.5 mm and 2.5 mm. Figure 6.5 shows the calculated gross interception in its top plot.

Stemflow is estimated from gross precipitation using a stemflow factor. Stemflow plus throughfall form the water input to the forest floor. When the forest floor exceeds its infiltration capacity, excess water becomes surface runoff. Infiltration enters the unsaturated soil layer, where evaporation and transpiration occur. When soil moisture exceeds field capacity, drainage begins into the deeper soil. Hydrological principles included here are: drainage increasing above field capacity, leakage continuing below it, evaporation scaling with soil moisture, and transpiration only occurring above the wilting point. Deep soil drains slowly over time.

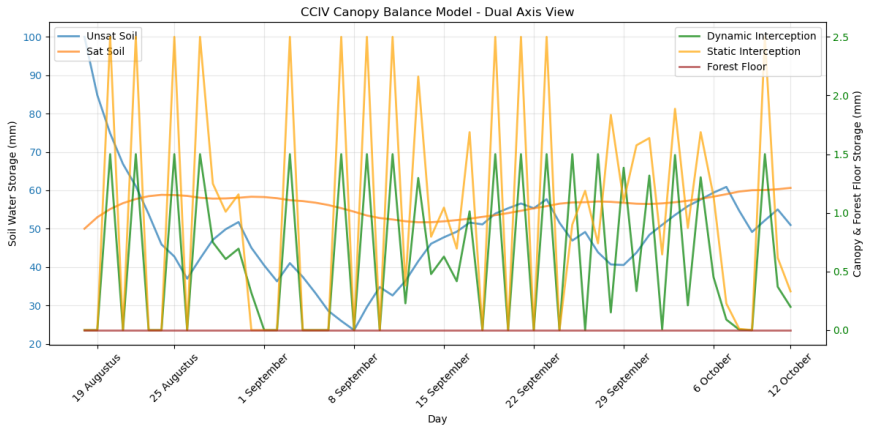

Figure 6.6.: Results from the canopy balance model.

Figure 6.6 shows of the canopy balance model. While not every storage component can be directly validated, the absence of unrealistic spikes or contradictory trends suggests that the forcing data are internally consistent. The forest floor component appears to not be functioning properly, future versions of the model should aim to improve the functioning of the forest floor storage variable.

Figure 6.7 shows soil moisture measured by the sensors at the tower. The top sensor is located at a depth of 0.1 meters and the bottom sensor at a depth of 0.3 meters. Both sensors behave similarly but have a near constant offset, suggesting redundancy. The data exhibit the expected pattern: gradual drying with sharp increases following rainfall.

Figure 6.7.: Soil moisture recorded by the two sensors at the tower.

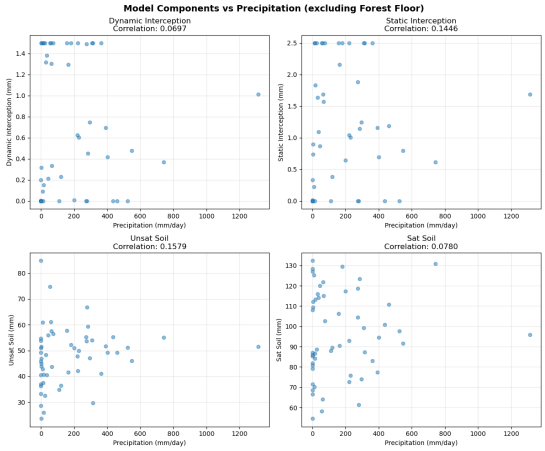

Figure 6.8.: Correlations between model storage components and precipitation.

Given that the period marks the onset of the rainy season, deep soil moisture gradually accumulating while the upper layer responds to daily fluctuations is consistent with expectations. Figure 6.9 shows that the modelled unsaturated soil moisture follows the same trend as the measured soil moisture. For figure 6.9 we normalized all input values to be able to reflect solely on their relationship, we see here that the modeled unsaturated soil follows the sensor data rather well. Its initial value was likely set too high, causing an initial normalized decrease but later during the time series it seems to follow the measured data rather well. The saturated soil variable displays a more rounded profile which is consistent with the physical behavior we expect from it. Overall, figure 6.8 indicates that the modeled soil moisture variables follow the trend in the measured variables. This is an indicator that the canopy balance model can be used to predict and accurately model hydrological processes.

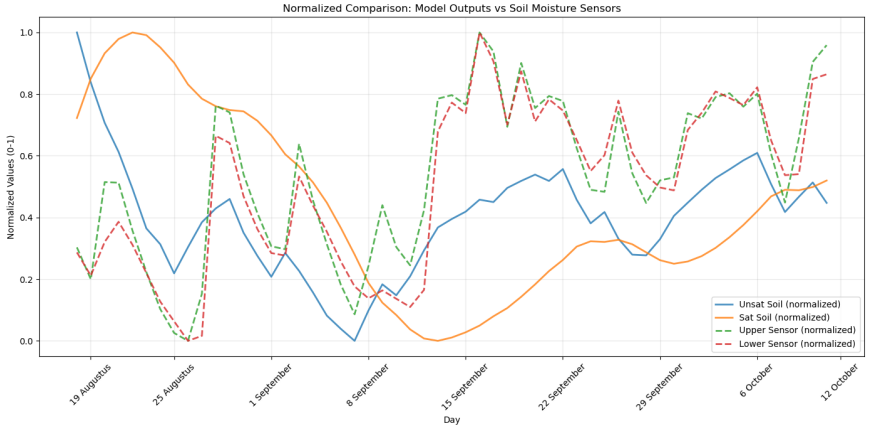

Figure 6.9.: Normalized soil moisture for the sensors and the canopy balance model.

6.3. Meteorological comparison

We now compare weather station data from the tower and the cabin. This comparison focuses on September, as tower data quality declined afterwards. Our goal is to understand systematic differences between the two stations.

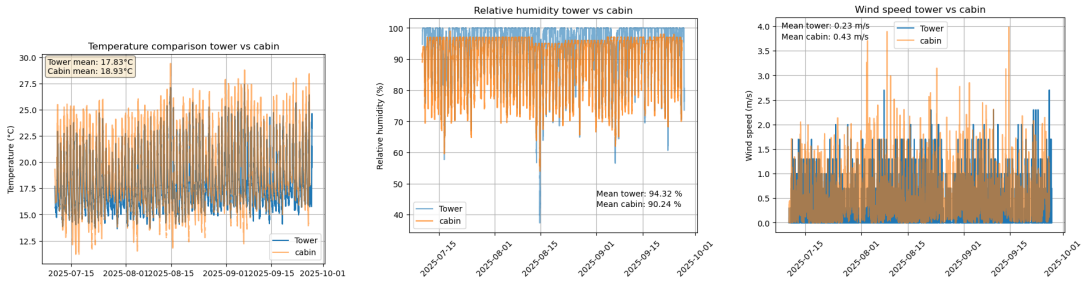

(a) Temperature (b) Relative humidity (c) Wind speed

Figure 6.10.: Comparison of three main weather variables between the tower and cabin stations.

Figure 6.10 shows that the tower consistently records lower temperatures and higher relative humidity — expected given its location inside the cloud forest rather than in an open field. This was also discussed in section 4.1.

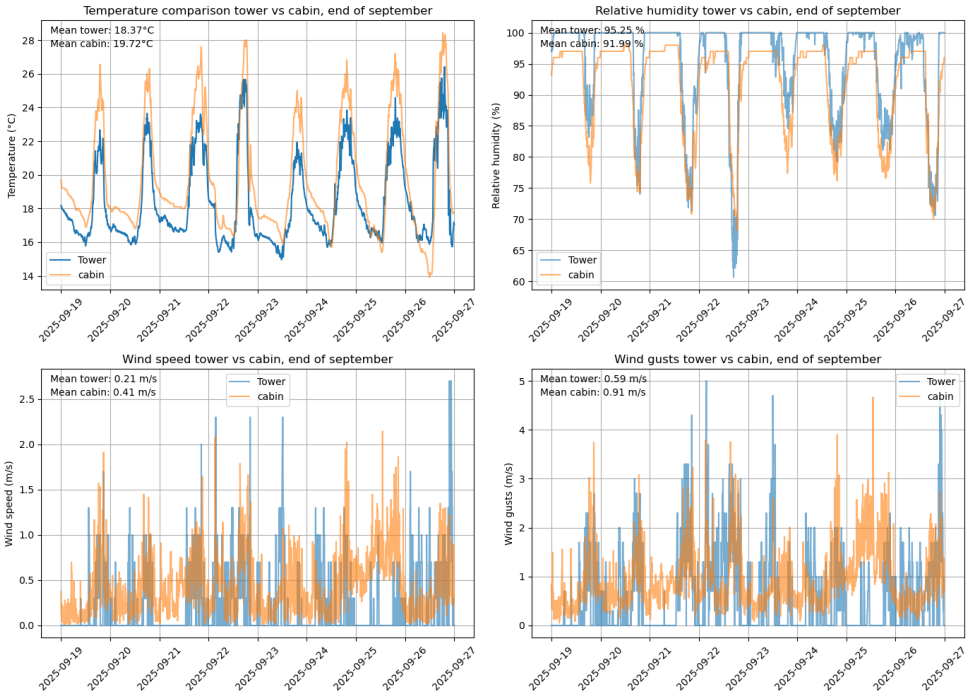

Figure 6.11.: One-week comparison between the tower and cabin stations.

Figure 6.11 shows that diurnal temperature and humidity cycles differ as well, with reduced temperature peaks and prolonged humidity at the tower site. This reflects the cooling and buffering effect of the canopy.

The two stations differ by an average of 1.1 °C in temperature, with the cabin station warmer. Given the 200 m elevation difference and the contrasting land-use types, this difference is lower than expected. In our FIESTA modelling we assumed a cooling effect of -0.6 degrees Celsius per 100 meters of elevation increase. Additionally our data shows that daytime temperatures in Cloud Forest land use area were approximately 1.8 degrees Celsius cooler. Combining these two differences would mean that a larger difference than 1.1 degrees Celsius should be observed. Figure 6.11 additionally also shows that the average difference in relative humidity between the two weather stations is around 4%. Looking back at section 4.1 we observe that we would expect these differences to be bigger based on our own LogTag measurements. Our LogTag measurement predict around a 7% diffrence in daytime relative humidity between Cloud forest and Pine forest. Since the cabin weather station is located in a more open field setting we would expect this difference to be even bigger.

These differences underscore the necessity for more measurements and understanding of how meteorological conditions depend on land use, elevation and other factors. This is underscored by the relative closeness of the two weather stations. The stations are only about 500m apart (Figure 6.12). A better understanding of how microclimates behave under different spatial and temporal factors would positively impact our understanding of the hydrological cycle too.

Figure 6.12.: Google Earth image showing the distance between the stations.

6.4. Conclusion

The canopy balance model, when driven by tower measurements, reproduces the expected behaviour of a cloud forest at the start of the rainy season. The gradual rise of the deep soil

store and the buffered response of the unsaturated layer align with both hydrological principles and the soil moisture sensors at the tower. One component, the forest floor storage, remains non-functional in its current form and will require redesign in future iterations.

Our analysis of fog events shows that horizontal precipitation behaves independently from rainfall and cannot be inferred from a standard rain gauge alone. The timing differences observed between fog interception, precipitation and throughfall confirm the necessity of dedicated in-canopy instrumentation for characterizing cloud immersion.

The comparison between the cabin and tower weather stations demonstrates that microclimate varies substantially over short distances due to land-use type, canopy cover and elevation. The cabin station cannot reliably represent conditions inside the cloud forest, underscoring the value of using tower data for spatially explicit hydrological modelling. The unexpectedly small differences in temperature and relative humidity between the two stations also indicate that additional measurements are needed to resolve land-use and elevation effects.

To refine the canopy balance model and improve the spatial performance of FIESTA, future work should include installing a weather station in a pine stand, assessing elevation gradients more systematically, and improving the representation of forest floor processes. Together, these steps would strengthen the ability of the modelling framework to capture hydrological variation across the CCFC landscape.

7. Continuation and Further Research

The work carried out in this project represents an important step in advancing the long-term Cloud Chasers research effort in collaboration with Community Cloud Forest Conservation (CCFC). By developing a tailored land-use classification, constructing high-resolution spatial inputs, and adapting meteorological data for use in the FIESTA fog interception model, this study has created a foundation upon which future research teams can build. Nevertheless, both the complexity of the Sierra Yalijux cloud forest environment and the exploratory nature of this modeling effort leave significant room for scientific expansion. The following discussion outlines key directions for continuation, integrating computational, ecological, and hydrological components, as well as opportunities for deeper field engagement.

Following the project presentation in Guatemala, feedback from practitioners highlighted several practical considerations for future work. Representatives from CONAP (Consejo Nacional de Áreas Protegidas, Guatemala's national authority responsible for protected areas and biodiversity conservation) emphasized that long-term cloud forest protection depends on environmental education and community involvement alongside technical monitoring. It was further stressed that restoration cannot rely solely on replanting cloud forest species; instead, regenerative agriculture and agroforestry were identified as more feasible pathways that allow environmental protection without compromising local livelihoods. Additionally, CONAP advised that future hydrological studies could benefit from using ArcGIS for river-network and tributary analysis, as its hydrology toolsets may provide improved tracing and flow-path functionality compared to QGIS.

A first area where subsequent research can meaningfully contribute lies in improving the spatial characterization of the watershed. Although the land-use classification built for this project successfully distinguished between pine plantations, cloud forest, and agricultural areas, it remains constrained by the limitations of satellite imagery alone, particularly given the persistent cloud cover over the region and the spectral similarity between shadowed cloud forest and mature pine. Multi-season imagery or higher-resolution data could therefore help resolve ambiguities in vegetation type and improve the dynamic representation of agricultural cycles. Similarly, the availability of high-resolution elevation data derived from drone photogrammetry or LiDAR as seen in studies by Zhou and in image 7.1could significantly enhance slope, curvature, and canopy exposure estimates, all of which strongly influence fog deposition processes [45]. Complementary field surveys for instance, basic measurements of canopy height, understory density, or leaf area index would further allow future teams to refine the ecological parameters that determine interception efficiency within the FIESTA framework.

Meteorological forcing remains a second major source of uncertainty in fog interception modeling for montane tropical environments. This project relied on a combination of INSIVUMEH, LogTag, HOBO, and handheld weather data, but the spatial and temporal heterogeneity of the Yalijux suggests that a denser observational network is needed. Future teams could expand the distributed sensor array with additional temperature and humidity log tags placed strategically along elevational gradients to better capture the movement of

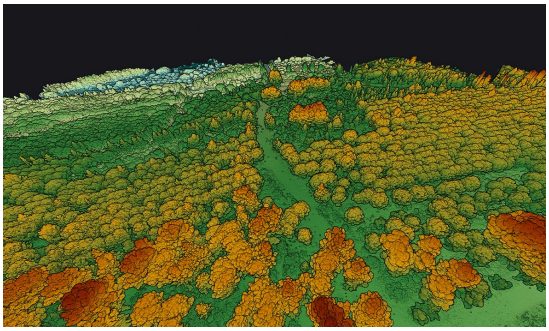

Figure 7.1.: YellowScan uses drone-mounted LiDAR systems to generate high-density 3D point clouds of forested landscapes, enabling accurate measurements of individual tree heights, canopy structure, vegetation density, and under-canopy terrain

the cloud base throughout the day. Leaf wetness sensors could provide direct detection of fog events, while simple anemometers placed along ridgelines or in forest clearings would help quantify wind-driven droplet fluxes. Radiation measurements would also help resolve energy-balance mechanisms that influence fog formation and dissipation. Together, such observations would greatly reduce the atmospheric uncertainties that currently propagate into FIESTA outputs.

The challenges encountered in measuring fog deposition on the ground further highlight the need for more robust and standardized fog monitoring equipment. Future research should therefore aim to standardize fog collectors ideally employing designs with known aerodynamic efficiencies and install replicated collectors across a range of elevations and topographic positions. In time, a coherent fog deposition dataset would enable rigorous calibration and validation of the FIESTA model for the Sierra Yalijux. Beyond atmospheric measurements, integrating hydrological field observations into the research program represents one of the most impactful opportunities that is feasible for other MDP groups. While fog deposition increases ecological water availability, the degree to which it influences streamflow and groundwater recharge remains unquantified. Installing simple staff gauges at strategic points along streams such as the Mestelá would allow future teams to conduct repeated stage measurements and develop rating curves that translate water level into discharge. Pressure-based water-level loggers could provide continuous monitoring of stream fluctuations throughout the dry and wet seasons. Soil moisture transects whether measured using capacitance probes could reveal how different land-cover types (pine, cloud forest, agriculture) retain and transmit fog-derived moisture. Basic shallow piezometers, constructed from PVC, could further illuminate groundwater responses to fog events. Such measurements would collectively enable the first characterization of how fog water propagates through the hydrological system of this rare mountain cloud forest.

Improving cloud-base height estimation also represents a promising avenue. This project relied primarily on a simplified lifted condensation level (LCL) calculation based on temperature and humidity, yet field conditions in complex terrain often deviate from theoretical behavior due to thermal inversions, cold-air pooling, and orographic lifting. As shown in recent studies, perhaps the utilization of ConvLSTM-XGBoost hybrid model would provide a basis that could better handle the complexity of this microclimate [46].

From a modeling perspective, this project builds upon the existing FIESTA model developed

by L. Adrian Bruijnzeel et al. and modified for Jolijn Hiemstra's Masters thesis for Assessment of local land cover change on the streamflow dynamics in tropical montane cloud forest region. We built upon this and developed new preprocessing routines, calibrated land-use classes for a tropical montane environment, and integrated distributed meteorological data into a format compatible with FIESTA's computational structure. Future research teams have the opportunity to continue this trajectory by coupling FIESTA outputs with more comprehensive hydrological models such as FLEXTopo to simulate full watershed water balances, though it has been attempted before with cloud chasers VI better integration and data would would enable the local community to evaluate long-term effects of land-use change on water availability. Thereby linking ecological restoration to hydrological outcomes.

Finally, the success of the Cloud Chasers initiative depends not only on scientific progress but also on deepening engagement with local communities and strengthening local agency in environmental monitoring. Future teams can play an important role by co-developing educational materials with CCFC staff and students, training youth in the use of meteorological sensors, GIS tools, and stream measurement techniques, and designing low-cost, easy-to-maintain monitoring systems that can be left in place after field teams depart. Through these efforts, the scientific insights generated by the project can directly support CCFC's conservation mission and empower local stewards of the cloud forest.

In a conversation with Luis, one of the local biologists it came to light that there is of course ongoing cloud forest conservation efforts within the country but there is a lack of sufficient research in the area to support conservation efforts. Together, these research directions outline a pathway toward a fully integrated understanding of fog, vegetation, and hydrology in the Sierra Yalijux. By combining improved spatial mapping, expanded sensor networks, enhanced fog monitoring, and direct hydrological measurements, future teams have the opportunity to transform this exploratory modeling effort into a comprehensive scientific framework that informs conservation planning and protects one of the world's most threatened ecosystems.

8. Conclusions

This study demonstrates that land-use change in tropical montane environments has direct and measurable impacts on atmospheric processes that control cloud formation and fog interception. Using a distributed sensor network in the Mestelá catchment, clear differences in microclimate were observed between cloud forest, pine forest, and agricultural land. These differences translated consistently into variations in cloud base height.

Cloud forests maintained the coolest and most humid conditions, allowing for the lowest cloud base heights and the highest potential for fog interception. Pine forests showed intermediate behavior, while agricultural areas produced significantly warmer, drier conditions and elevated cloud bases. This confirms the hypothesis that deforestation and land conversion contribute to shifting cloud formation upward, reducing forest immersion frequency and weakening a key hydrological function of the ecosystem.

Incorporating observed microclimatic differences and increasing temporal resolution into the FIESTA model improved fog interception representation and demonstrated how changes in land cover influence water inputs at catchment level. Canopy water balance results further showed that fog contributes meaningfully to moisture availability, even during the rainy season, and is likely critical in dry periods. Furthermore, comparing data between two weather stations on the CCFC campus further shows how important it is to understand microclimate variability.

The implications of these findings extend beyond atmospheric science. In a region where communities rely heavily on untreated surface water and forest-fed springs, altered cloud dynamics may exacerbate water shortages and increase vulnerability to climate change. Continued deforestation therefore represents not only an ecological risk, but a socioeconomic threat.

From a methodological perspective, this project shows that low-cost sensor networks can effectively capture atmospheric gradients in remote environments and provide valuable insights into climate–land interactions. The combination of field measurement and modeling presented here offers a transferable framework for other cloud forest regions. However, doing longer-term measuring of meteorological conditions over the different types of land-uses could help increase understanding and also accuracy of modelling results. This could be done by installing weather stations within the CCFC campus one different sites.

Future research should expand temporal coverage to include dry seasons, integrate cloud base height directly into fog-interception models, and incorporate satellite-based cloud observations for validation. In addition, stronger collaboration with local communities and policymakers is essential to link scientific insight to sustainable land management.

Ultimately, preserving cloud forests is not merely an act of conservation, but a form of water infrastructure protection.

A. Radiation Shield testing

For the radiation shield testing, 8 different designs and 2 controls have been tested. They are given in this appendix and briefly explained. (Nog even netter uitwerken aub misschien iets meer text ook nog)

LogTag A

A single LogTag placed in an open grass field, sparsely surrounded by vegetation. This unit serves as the humidity control.

Honeycomb B

For the honeycomb design, the top cover is the upper part of a Coca-Cola bottle; below it sits a circular plate with some holes. This configuration should reflect radiation effectively, but may perform less well for humidity.

R2D2 C

This design uses a small dome on top and a single plastic band cut from a Coca-Cola bottle, fixed with duct tape, as the radiation shield.

Small Collin D

A small funnel through which the pulley rope just fits. The funnel itself is not wrapped in aluminium foil to test for other effects. Beneath the funnel, three rings of chicken wire are tightly wrapped with aluminium foil.

Big Collin E

A scaled-up variant of the Small Collin; here the funnel is also wrapped in aluminium foil.

Leaf Foil Johannes F

A horizontal layer of chicken wire on the top side with leaves attached underneath, integrating natural material into the shield. This is a basic, easy-to-produce design.

Dome G

An inverted basket with the exterior of the top covered in aluminium foil. Expected to shield well against radiation, but ventilation is limited.

Inside H

The LogTag is placed in the shade of the large porch of the house. Used for comparison of the air temperature.

Jellyfish Alma I

A flat, disc-like top with vertical strands below. Intended to compare ventilation via vertical gaps versus horizontal gaps.

Foil Bob J

Similar to Leaf Foil Johannes but with fewer leaves beneath the shield, to reduce the risk of retained water artificially elevating humidity.

(a) LogTag A

(b) Honeycomb B

(c) R2D2 C

(d) Small Collin D

Figure A.1.: Radiation shield designs (A–D).

(a) Big Collin E

(b) Leaf Foil Johannes F

(c) Dome G

(d) Inside H

Figure A.2.: Radiation shield designs (E–H).

(a) Jelly Fish Alma I (b) Foil Bob J

Figure A.3.: Radiation shield designs (I–J).

B. LogTag deployment locations

This appendix explains in more detail, the surroundings of each LogTag location. The sites are discussed in more detail, aswell as the challenges related to installing the LogTags. For every site a vegetation density is given (dense, moderately dense, open) and the installation heights of the LogTags are presented in the corresponding table.

B.1. Cloud and Pine Forests: comparison by altitude (Batch 1)

The first batch of LogTags were to compare the impact of altitude on temperature and humidity in cloud and pine forest.

B.1.1. Cloud Forest

The first tree used was located in the low cloud forest, close to the base of operations for this project. It stood in a smaller patch of cloud forest. The main challenge in selecting this tree was finding one within a dense area, while ensuring that a suitable branch was available. The branch needs to be unobstructed and high enough for placement. Eventually, the tree shown in Figure B.1 was selected, which was well position, right above a path in the cloud forest.

The second tree was more difficult. It was located at a higher altitude, on a slope just off the path. This area was much denser, making it harder to reach higher branches. An image of this tree, for visual reference, is provided in Figure B.2. The heights at which the LogTags were installed for data collection are listed in Table B.1.

Table B.1.: LogTag heights: Altitude Comparison, Cloud Forest

Position	**Cloud Forest (Low)** **B1CF1**	**Cloud Forest (High)** **B1CF2**
Top	14.0 m	11.0 m
Middle	8.0 m	5.0 m
Bottom	0.5 m	0.5 m

Figure B.1.: Cloud Forest Low

Figure B.2.: Cloud Forest High

B.1.2. Pine Forest

The second set of locations regarded the pine forest. Around CCFC, a large restoration operation is taking place. Half of the pine trees on the pine forest patches on CCFC's land are being removed to allow for the restoration of cloud forest. In a later phase of the project, the remaining half of the pine forest will also be cleared, leading to full restoration of cloud forest vegetation.

This context is important, as it means that the current pine forest patches are only moderately dense. The restoration process is still ongoing, and the new cloud forest has not yet been planted, which makes it somewhat easier to reach greater heights for positioning the LogTags. This was also the case for the low pine forest site, where the placement was high but relatively open, as shown in Figure B.3.

At the high pine forest site, the terrain was again on a slight slope, which made the setup more challenging. In addition, the pine trees had multiple branches, making it more difficult to reach higher placements. The installation heights of the LogTags are listed in Table B.2.

B.2. Ariel's Farm (Batch 2)

The second batch of LogTags were deployed at Ariel's Farm. Ariel's Farm is also in the Mestelá catchment, only a few more kilometers upstream. The great thing about the farm is that all 3 sorts of main vegetation are present: agricultural field, pine forest and native forest.

Figure B.3.: Pine Forest Low

Figure B.4.: Pine Forest High

Table B.2.: LogTag heights: Altitude Comparison, Pine Forest

Position	**Pine Forest (High) B1Pine1**	**Pine Forest (Low) B1Pine2**
Top	11.0 m	21.0 m
Middle	5.7 m	14.0 m
Bottom	0.5 m	0.5 m

B.2.1. Ariel: Agricultural Field

The first vegetation site was the agricultural field. In between the cows, the LogTags had to be installed in the trees. Ideally, the LogTags should be placed as high as possible, while avoiding placement inside the canopy. Suitable trees therefore needed to be isolated among the cattle. For the agricultural field, two suitable trees were found. An impression of the site is provided in Figure B.5. The installation heights of the LogTags are listed in Table B.3.

Table B.3.: LogTag heights: Ariel, Agricultural Field

Position	B2Agro1	B2Agro2
Top	4.7 m	6.5 m
Middle	2.7 m	3.5 m
Bottom	0.7 m	0.5 m

Figure B.5.: Ariel Agricultural Field

B.2.2. Ariel: Pine Forest

Figure B.6.: Ariel Pine Forest

The second batch focused on the pine forest. This was a particularly dense patch, quite different from the area used in the altitude comparison at CCFC's ground.

A major disadvantage of the pine plantation on Ariel's farm was the large number of small branches on each tree. With the system used, the pulley could only be attached to the lowest available branch, as higher branches would make the pulley become tangled. This led to the heights of the LogTags being lower than those in the pine forest sites used for the altitude comparison.

Table B.4.: LogTag heights: Ariel, Pine Forest

Position	B2Pine1	B2Pine2
Top	7.7 m	7.7 m
Middle	3.7 m	4.7 m
Bottom	0.2 m	0.7 m

B.2.3. Ariel: Native Forest

The third and final location on Ariel's farm was the native forest. This site was the most distant from the farm's starting point. Ariel's property contained only small patches of native forest, all of which were very dense. Within this particular patch, only one tree was selected, as it was considered to be sufficient given the limited size of the area. It was a challenging setup, but one of the taller trees within the native forest patch was successfully used for the installation.

Table B.5.: LogTag Heights: Ariel, Native Forest

Position	**B2CF1**
Top	14.0 m
Middle	7.0 m
Bottom	0.5 m

Figure B.7.: Native Forest

B.3. Ariel's Farm Revisited (Batch 3)

Since the sites at Ariel's Farm proved well suited for the investigation, one of the trees at each site was removed, and one sensor was taken down from the remaining tree. The remaining sensors were left in place to continue data collection. An overview of the sensors still installed is provided in Table B.6.

Table B.6.: LogTag heights: Ariel's Farm 3rd batch

Position	**Agricultural Field B3Agro1**	**Pine Forest B3Pine1**	**Native Forest B3CF1**
Top	4.7 m	7.7 m	14.0 m
Middle	-	-	7.0 m
Bottom	0.7 m	0.2 m	-

B.4. CCFC: Cloud Forest, Pine Forest & Open Field (Batch 4)

For the 4th batch we decided to gather more data around CCFC. Since there are 6 LogTags up at Ariel's Farm, we had 12 LogTags to spread over 5 locations: 2 cloud forest locations, 2 pine forest locations and 1 open field location.

B.4.1. CCFC: Cloud Forest

In the cloud forest, a new type of distinction was introduced by selecting two trees located less than 100 meters apart. One tree situated in an area with very dense vegetation and the other in a more open part of the forest. Images of both the trees are shown in Image B.8 and B.9. Because of the height of the open tree and the way it was located on a hill, measurements could be taken which are slightly above some canopy. The dense-area tree was located in thick vegetation, which made it harder to get sufficient height for the shot. The heights of the LogTags are provided in Table B.7.

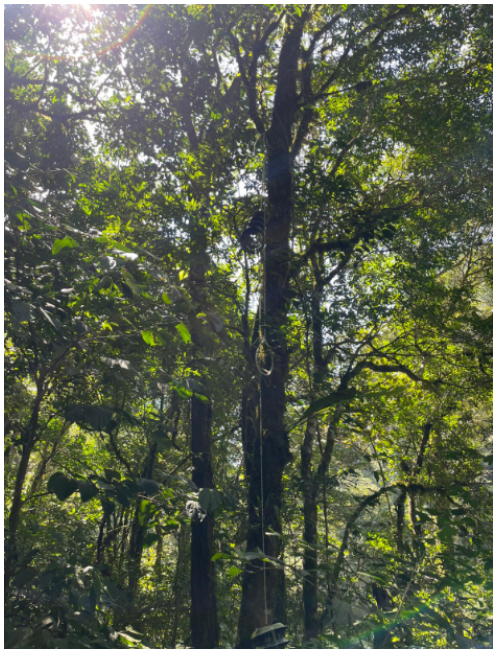

Figure B.8.: Cloud forest dense

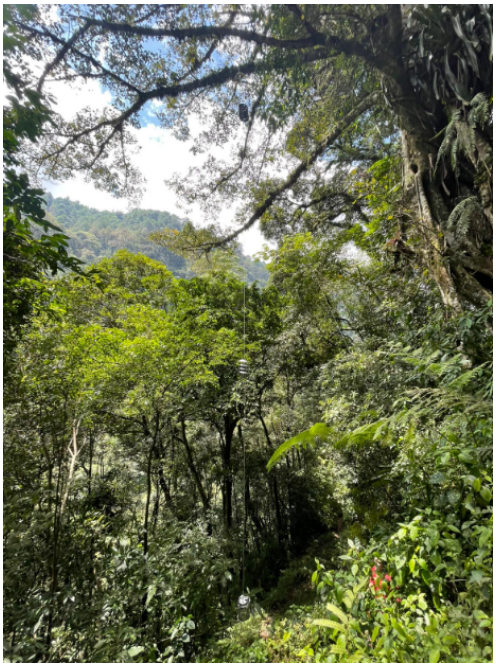

Figure B.9.: Cloud forest open

Table B.7.: LogTag heights: CCFC Cloud Forest

Position	**Cloud Forest (Dense) B4CF1**	**Cloud Forest (Open) B4CF2**
Top	6.0 m	12.0 m
Middle	3.0 m	6.0 m
Bottom	-	1.0 m

B.4.2. CCFC: Pine Forest

For the two pine trees, there was only a small difference in altitude. The lower pine tree is located on the same patch as the low pine tree from Batch 1 (B1Pine2), while the higher one is situated on a new patch along the hillside on the west side of CCFC, near the location of

B1Pine1. The heights of the LogTags are shown in Table B.8. Images B.10 and B.11 illustrate the sites. The Pine Forest Low area is open, with a little undergrowth and wide tree spacing. The Pine Forest High is **explain**

Figure B.10.: Pine Forest Low

Figure B.11.: Pine Forest High

Table B.8.: LogTag heights: CCFC Pine Forest

Position	**Pine Forest (High)** **B4Pine1**	**Pine Forest (Low)** **B4Pine2**
Top	14.0 m	20.0 m
Middle	7.0 m	-
Bottom	0.0	0.5 m

B.4.3. CCFC: Open Field

Around CCFC, there are also some open fields, where often sheep can be seen. This open area is interesting, because it lies at the bottom of a valley, surrounded by both cloud forest and pine forest. Within this open field, a suitable tree was selected to attach two LogTags. Since no pulleys were available, the sensors were installed with solely a rope in the tree. The purpose of this setup was to gain additional insight into the open-field conditions in this area, as a comparison to the agricultural field at Ariel's Farm. The heights are given in Table B.9.

Table B.9.: LogTag heights: CCFC Open Field

Position	B4Agro1
Top	9.0 m
Middle	-
Bottom	0.0 m

B.5. CCFC 2 (Batch 5)

For the 5th and final batch the objective was to take home as much data as possible. The 6 LogTags that were left after taking them from Batch 3 (Ariel's Farm Revisited) were now deployed in other areas around CCFC. The 2 locations with each 2 LogTags for Cloud Forest trees, had been spotted some time ago, when hiking to the tower built by Cloud Chasers IV. The location for the pine tree was right behind the CCFC building. Here used to be a big patch of pine forest, but recently half of the pines had been removed and cloud forest is being restored. Therefor, significant undergrowth was present, as can be seen in Image B.12c. The LogTag heights are shown in Table B.10.

Table B.10.: LogTag heights: CCFC 2

Position	Cloud Forest Tower 1 B5CF1	Cloud Forest Tower 2 B5CF2	Pine Forest B5Pine1
Top	10.0 m	8.0 m	11.0 m
Middle	-	-	-
Bottom	0.5 m	0.5 m	0.6

(a) Cloud Forest 1 (b) Cloud Forest 2 (c) Pine Forest

Figure B.12.: Trees final round of measurements

Bibliography

[1] Vincent S. F. T. Merckx, Kasper P. Hendriks, Kevin K. Beentjes, Constantijn B. Mennes, Leontine E. Becking, Katja T. C. A. Peijnenburg, Aqilah Afendy, Nivaarani Arumugam, Hugo De Boer, Alim Biun, Matsain M. Buang, Ping-Ping Chen, Arthur Y. C. Chung, Rory Dow, Frida A. A. Feijen, Hans Feijen, Cobi Feijen-Van Soest, József Geml, René Geurts, Barbara Gravendeel, Peter Hovenkamp, Paul Imbun, Isa Ipor, Steven B. Janssens, Merlijn Jocqué, Heike Kappes, Eyen Khoo, Peter Koomen, Frederic Lens, Richard J. Majapun, Luis N. Morgado, Suman Neupane, Nico Nieser, Joan T. Pereira, Homathevi Rahman, Suzana Sabran, Anati Sawang, Rachel M. Schwallier, Phyau-Soon Shim, Harry Smit, Nicolien Sol, Maipul Spait, Michael Stech, Frank Stokvis, John B. Sugau, Monica Suleiman, Sukaibin Sumail, Daniel C. Thomas, Jan Van Tol, Fred Y. Y. Tuh, Bakhtiar E. Yahya, Jamili Nais, Rimi Repin, Maklarin Lakim, and Menno Schilthuizen. Evolution of endemism on a young tropical mountain. *Nature*, 524(7565):347–350, 8 2015.

[2] L. A. Bruijnzeel, Mark Mulligan, and Frederick N. Scatena. Hydrometeorology of tropical montane cloud forests: emerging patterns. *Hydrological Processes*, 25(3):465–498, 12 2010.

[3] L. Adrian Bruijnzeel, F. N. Scatena, and L. S. Hamilton. *Tropical Montane Cloud Forests: Science for Conservation and Management*. Cambridge University Press, Cambridge, UK, 2011.

[4] Edgar G. Leija-Loredo, Numa P. Pavón, Arturo Sánchez-González, Rodrigo Rodriguez-Laguna, and Gregorio Ángeles Pérez. Land cover change and carbon stores in a tropical montane cloud forest in the Sierra Madre Oriental, Mexico. *Journal of Mountain Science*, 15(10):2136–2147, 10 2018.

[5] Lawrence S. Hamilton. *A campaign for cloud forests : unique and valuable ecosystems at risk*. 1 1995.

[6] D. V. Spracklen and R. Righelato. Tropical montane forests are a larger than expected global carbon store. *Biogeosciences*, 11(10):2741–2754, 5 2014.

[7] Temesgen Alemayehu Abera, Janne Heiskanen, Eduardo Eiji Maeda, Mohammed Ahmed Muhammed, Netra Bhandari, Ville Vakkari, Binyam Tesfaw Hailu, Petri K. E. Pellikka, Andreas Hemp, Pieter G. Van Zyl, and Dirk Zeuss. Deforestation amplifies climate change effects on warming and cloud level rise in African montane forests. *Nature Communications*, 15(1):6992, 8 2024.

[8] Zhenzhong Zeng, Dashan Wang, Long Yang, Jie Wu, Alan D. Ziegler, Maofeng Liu, Philippe Ciais, Timothy D. Searchinger, Zong-Liang Yang, Deliang Chen, Anping Chen, Laurent Z. X. Li, Shilong Piao, David Taylor, Xitian Cai, Ming Pan, Liqing Peng, Peirong Lin, Drew Gower, Yu Feng, Chunmiao Zheng, Kaiyu Guan, Xu Lian, Tao Wang, Lang Wang, Su-Jong Jeong, Zhongwang Wei, Justin Sheffield, Kelly Caylor, and Eric F. Wood.

Deforestation-induced warming over tropical mountain regions regulated by elevation. *Nature Geoscience*, 14(1):23–29, 12 2020.

[9] Mi Zhang, Xuhui Lee, Guirui Yu, Shijie Han, Huimin Wang, Junhua Yan, Yiping Zhang, Yide Li, Takeshi Ohta, Takashi Hirano, Joon Kim, Natsuko Yoshifuji, and Wei Wang. Response of surface air temperature to small-scale land clearing across latitudes. *Environmental Research Letters*, 9(3):034002, 3 2014.

[10] R. O. Lawton, U. S. Nair, R. A. Pielke, and R. M. Welch. Climatic Impact of Tropical Lowland Deforestation on Nearby Montane Cloud Forests. *Science*, 294(5542):584–587, 10 2001.

[11] Martha A. Scholl, Maoya Bassiouni, and Angel J. Torres-Sánchez. Drought stress and hurricane defoliation influence mountain clouds and moisture recycling in a tropical forest. *Proceedings of the National Academy of Sciences*, 118(7), 2 2021.

[12] Wikipedia Alta Verapaz. Alta verapaz — wikipedia, de vrije encyclopedie, 2025. Accessed: 6 October 2025.

[13] Jolijn Hiemstra. Assessment of local land cover change on the streamflow dynamics in tropical montane cloud forest region, alta verapaz, guatemala. Master's thesis, Delft University of Technology, Delft, The Netherlands, October 2024. Faculty of Civil Engineering and Geosciences. Supervisors: Dr. S. Pande, Dr. M. Hatchikurc, and L. Chahil (CCFC).

[14] María A. Máñez Costa and Manfred Zeller. Peasants' production systems and the integration of incentives for watershed protection: A case study in guatemala. In *Proceedings of the International Conference on Rural Livelihoods, Forests and Biodiversity*, Bonn, Germany, May 2003. Topic 4: Improving livelihoods and protecting biodiversity.

[15] Community Cloud Forest Conservation. Q'eqchi' maya. https://cloudforestconservation.org/knowledge/community/qeqchi-maya/. Accessed: 2025-07-04.

[16] J. M. Vargas, F. Pérez-Arce, and S. Valdés-Prieto. Spatial analysis of poverty in guatemala: The case of alta verapaz department. *Economía, Sociedad y Territorio*, 16:291–322, 2016.

[17] Dawn S. Bowen, Jon Harbor, Guofan Shao, Laura Zanotti, et al. Deforestation of montane cloud forest in the central highlands of guatemala: Contributing factors and implications for sustainability in q'eqchi' communities. *International Journal of Sustainable Development & World Ecology*, 22(1):1–12, 2015.

[18] Swen C. Renner, Malte Voigt, and Michael Markussen. Regional deforestation in a tropical montane cloud forest in alta-verapaz, guatemala. *Ecotropica*, 12:43–49, 2006.

[19] Ali Akbar Firoozi and Ali Asghar Firoozi. Water erosion processes: Mechanisms, impact, and management strategies. *Current Opinion in Environmental Science & Health*, 2024.

[20] Cecilia Alfonso-Corrado, Francisco Naranjo-Luna, Ricardo Clark-Tapia, Jorge E. Campos, Octavio R. Rojas-Soto, María Delfina Luna-Krauletz, Barbara Bodenhorn, Montserrat Gorgonio-Ramírez, and Nelly Pacheco-Cruz. Effects of environmental changes on the occurrence of Oreomunnea mexicana (juglandaceae) in a biodiversity hotspot cloud forest. *Forests*, 14(5):1033, 2023.

[21] Mark Mulligan and Sophia M. Burke. Fiesta: Fog interception for the enhancement of streamflow in tropical areas. Final technical report, King's College London and AMBIOTEK, 2005. KCL/AMBIOTEK contribution to DFID-FRP project R7991.

[22] Yvonne Lea. The agricultural deities of q 'eqchi' mayas, tzuultaq'as: Agricultural rituals as historical obligation and avatar of the cultural reservoir in rural lanquín, alta verapaz, guatemala. *Journal of Ethnology and Folkloristics*, 12(2):49–63, 2018.

[23] Eric L. Bullock, Christoph Nolte, Ana L. Reboredo Segovia, and Curtis E. Woodcock. Ongoing forest disturbance in guatemala's protected areas. *Remote Sensing in Ecology and Conservation*, 6(2):141–152, 2020.

[24] Julia Petreshen. Fog presence and ecosystem responses in a managed coast redwood forest. Master's thesis, University of Minnesota, May 2021.

[25] Antonio Sánchez-Falfán, Manuel Esperón-Rodríguez, Juan Cervantes-Pérez, and Monica Ballinas. How important are fog and the cloud forest as a water supply in eastern mexico? *Water*, 15(7):1286, 2023.

[26] Susana Prada, Miguel Menezes de Sequeira, Celso Figueira, and Manuel Oliveira da Silva. Fog precipitation and rainfall interception in the natural forests of madeira island (portugal). *Agricultural and Forest Meteorology*, 149:1179–1187, 2009.

[27] E. H. Helmer, E. A. Gerson, L. Scott Baggett, Benjamin J. Bird, Thomas S. Ruzycki, and Shannon M. Voggesser. Neotropical cloud forests and páramo to contract and dry from declines in cloud immersion and frost. *PLOS ONE*, 14(4):e0213155, 2019.

[28] Curtis D. Holder. The hydrological significance of cloud forests in the sierra de las minas biosphere reserve, guatemala. *Geoforum*, 35(5):689–701, 2004.

[29] Ashley E. Van Beusekom, Grizelle González, and Martha A. Scholl. Analyzing cloud base at local and regional scales to understand tropical montane cloud forest vulnerability to climate change. *Atmospheric chemistry and physics*, 17(11):7245–7259, 6 2017.

[30] Santiago Ramírez-Barahona, Ángela P. Cuervo-Robayo, Kenneth J. Feeley, Andrés Ernesto Ortiz-Rodríguez, Antonio Acini Vásquez-Aguilar, Juan Francisco Ornelas, and Hernando Rodríguez-Correa. Upslope plant species shifts in Mesoamerican cloud forests driven by climate and land use change. *Science*, 387(6738):1058–1063, 3 2025.

[31] Mark G Lawrence. The relationship between relative humidity and the dewpoint temperature in moist air: A simple conversion and applications. *Bulletin of the American Meteorological Society*, 86:225 – 234, 2 2005.

[32] Roland Stull. *Practical Meteorology: An Algebra-based Survey of Atmospheric Science*. University of British Columbia, version 1.02b edition, 2017.

[33] S. R. de Roode. 'the surface energy balance' [lecture notes], envm1800: Atmospheric measurements and modelling., 3 2025.

[34] L Bruijnzeel, Reto Burkard, Alexander Carvajal, Arnoud Frumau, Lars Köhler, Mark Mulligan, Jaap Schellekens, Simone Schmid, Conrado Tobon, Sophia Burke, Julio Calvo-Alvarado, and Jorge Fallas. Final technical report dfid-frp project no. r7991 hydrological impacts of converting tropical montane cloud forest to pasture, with initial reference to northern costa rica. Technical report, January 2006.

[35] S. Nicli et al. Socio-economic, political, and institutional sustainability of agroforestry in alta verapaz, guatemala. *DOAJ (Directory of Open Access Journals)*, 2019. Preprint.

[36] Amy Quandt, Henry Neufeldt, and Kayla Gorman. Climate change adaptation through agroforestry: Opportunities and gaps. *Current Opinion in Environmental Sustainability*, 60:101244, 2023.

[37] Ministerio de Agricultura, Ganadería y Alimentación (MAGA). Plan operativo anual 2017: Reprogramación. Technical report, Ministerio de Agricultura, Ganadería y Alimentación (MAGA), Guatemala City, Guatemala, 2017. Accessed: 26 November 2025.

[38] FAO. Sustainability pathways: Environment, economy, social, governance — did you know?, 2012. Food and Agriculture Organization of the United Nations (FAO).

[39] World Inequality Database. Guatemala – country profile. https://wid.world/country/guatemala/, 2025. Accessed: 2025-11-30.

[40] Maynor Cabrera, Nora Lustig, and Hilciás E. Morán. Fiscal policy, inequality, and the ethnic divide in guatemala. *World Development*, 76:263–279, 2015.

[41] Van Essen Instruments. *TD-Diver DI8xx Product Manual*, 2024. Accessed: 6 October 2025.

[42] Julia Brink, Job Stevens, Marloes Kragtwijk, Kaatje Bout, Eliane van Boxtel, Yoselin Marisol Quib Bac, Sara Elvira Caz Si, and Luis González. Establishing a long-term hydrological monitoring tower in the cloud forest of the mestelá river catchment. Cegm3000 multidisciplinary project report, TU Delft, Faculty of Civil Engineering and Geosciences, Delft, The Netherlands, June 2025.

[43] Zachary A. Holden, Anna E. Klene, Robert F. Keefe, and Gretchen G. Moisen. Design and evaluation of an inexpensive radiation shield for monitoring surface air temperatures. *Agricultural and Forest Meteorology*, 180:281–286, 2013.

[44] Jie Yang, Quan An, Qingquan Liu, Mengqing Tan, and Lixia Jiang. Development of a radiation shield for atmospheric temperature measurement system. *Measurement*, 229, 2024.

[45] L. Zhou et al. Comparison of uav-based lidar and digital aerial photogrammetry for measuring crown-level canopy height in the urban environment. *Urban Forestry & Urban Greening*, 69:127489, 2022.

[46] Yanting Dai et al. High-resolution climate prediction in mountainous terrain using a convlstm–xgboost hybrid model with dynamic bayesian weighting. *Scientific Reports*, 15(1):36923, 2025.

Colophon

This document was typeset using LaTeX, using the KOMA-Script class `scrbook`. The main font is Palatino.